Rheological profile of graphene-based nanofluids in thermal oil with hybrid additives of carbon nanotubes and nanofibers

Suhaib Umer Ilyas, Rashid Shamsuddin, Tan Kai Xiang, Patrice Estellé, Rajashekhar Pendyala

Rheological Profile of Graphene-based Nanofluids in Thermal Oil with Hybrid Additives of Carbon Nanotubes and Nanofibers

Suhaib Umer Ilyas [a,b 1], Rashid Shamsuddin [a, c 2], Tan Kai Xiang [a, d], Patrice Estellé [e 3], Rajashekhar Pendyala [a]

[a] Chemical Engineering Department, Universiti Teknologi PETRONAS, 32610 Seri Iskandar, Perak Darul Ridzuan, Malaysia
[b] Department of Chemical Engineering, University of Gujrat, 50700 Jalalpur Jattan Road, Gujrat, Pakistan
[c] HICoE-Centre for Biofuel and Biochemical Research, Institute for Self-Sustainable Building, Universiti Teknologi PETRONAS, 32610 Seri Iskandar, Perak Darul Ridzuan, Malaysia.
[d] Micron Memory Malaysia Sdn. Bhd., 14110 Bandar Cassia, Penang, Malaysia
[e] Univ Rennes, LGCGM, 35000 Rennes, France

Corresponding Authors: [1] suhaibui@gmail.com; [2] mrashids@utp.edu.my; [3] patrice.estelle@univ-rennes1.fr

Abstract

The evolution in nanofluid technology in the last few decades has proved the prodigious potential in several applications, especially thermal management and lubrication. An extensive investigation of nanofluid's rheological profile is vital to characterize the fluid flow behavior. This study signifies the rheological aspects of graphene and its hybrid nano-dispersions in thermal oil. The experimental investigation involves three sets of nanofluids containing graphene, graphene-carbon nanotubes, and graphene-carbon nanofiber hybrid nanofluid dispersions in thermal oil with varying loadings (0-2 mass%). The flow behaviors of all sets of nanofluids are measured at a wide shear range of 1-2000s^{-1} and five different temperatures from 298 K to 338 K. The morphology and stability are validated by performing several characterizations for nanomaterials and nanofluids. Non-Newtonian fluid behavior is observed in all nanofluids. This study reveals a few interesting outcomes where the fluid behaving as a Power Law model is shifted to the Herschel-Bulkley model at high loadings of nanomaterials. A comparative analysis illustrates that both hybrid additives act as viscosity reducers for graphene-based nanofluids, where graphene-carbon nanofibers hybrid nanofluids exhibit noticeable reduction. A parametric analysis is performed on the viscous behavior involving the impact of shear rate, temperature, nanomaterial loading, and surfactant concentration. The increment in viscosity shoots up to 180% for graphene-nanofluid at the 2000s^{-1} shear rate and 338 K temperature, but still exhibits shear thinning phenomena. A correlation is also proposed for the nanofluid viscosity in terms of nanomaterial loading and temperature, indicating a good agreement at varying shear rates.

Keywords

Carbon Nanofibers; Carbon Nanotubes; Graphene; Hybrid; Nanofluids; Rheology; Thermal oil.

1. Introduction

The miniaturization of devices requires advanced forms of heat transfer processes. Several research groups have been focusing on application-based nanofluid technology for two decades due to its significant potential in energy conservation and management [1]. The addition of nano-scale particles in the fluid media has opened new proficient capabilities in thermal management systems [2]. The nanofluid technology is not limited to heat transfer augmentation, but it has also demonstrated significant potential in a wide range of applications such as contaminant management, hydrocarbon recovery, pharmaceutical processes, fuel cells technology, lubricants, pigments, hybrid engines, refrigeration, machining, etc.[3–9].

Fluid's thermal conductivity is certainly increased with the inclusion of nanomaterials. However, it leads to an increase in effective viscosity and effective density, hence, exhibiting an adverse impact on heat transfer operations [10,11]. In several recent studies, a new trend of hybrid nanofluids has emerged where a combination of two nanomaterials with different properties are included in the nanofluid system [12,13]. Combining two nanomaterials in the hybrid systems can either be chemically bonded or mechanically added individual nanomaterials separately into the thermofluid. The primary purpose of developing a hybrid nanofluid system is to tune the thermophysical properties depending on the application requirement [14]. The existing literature is mainly dedicated to the thermal transport of the nanosuspensions, and little attention is focused on other associated thermophysical properties, such as rheology, heat capacity, surface tension, and thermal expansion coefficient. Therefore, there is a need to investigate different aspects of nanofluids that can demonstrate insightful understanding and improve the concept of nanofluid technology. Stability is also one of the strategic challenges in nanofluid technology, which must be measured quantitatively prior to the properties measurements, it is also termed as the validity of the nanofluids [15,16]. Several mechanical and chemical stabilization techniques are established in the literature [17–19], demonstrating promising results.

Thermal oils are widely used in heat transfer devices as heat dissipation media due to their high-temperature operability and lubricant characteristics. However, lower thermal conductivity is one of the major drawbacks of conventional thermal oils [20,21]. Nanofluid technology provides an impeccable solution to increase thermal conductivity by introducing metal-, non-metal-, or carbon-based nanomaterials. The addition of such nanomaterials alters all thermophysical properties relevant to heat and mass transfer, especially rheology. Rheology is an important characteristic, which can assess flow behavior. Many studies [22,23] have reported the shear effect on the viscosity of colloidal suspensions at

varying nanomaterial loadings and temperatures. Several studies have reported the non-Newtonian behavior of oil-based nanosuspensions [24–26], however, a few studies also reported the Newtonian phase [27–29] depending on the shear conditions and particle loading.

Carbonaceous nanomaterials are branded with high thermal conductivities that include graphene structure, nanotubes, and nanofibers. Graphene nanoplatelets (G) consist of mono-layer sp2-bonded carbon atoms, bounded in a hexagonal lattice. It has unique mechanical, thermal, optical, and energy storage properties. Graphene has demonstrated promising potential in several industrial applications, such as drug delivery, bio-imaging, sensors, electronic transistors, electrodes, photo-detectors, energy generation/storage, etc. [30–32]. Recently, graphene has proven attractive characteristics as a coolant additive [8,33] and lubricity agent [34,35]. Carbon nanotubes are cylindrical-shaped carbon structures with noteworthy applications in energy management, electronics, chemical processing, materials science, etc. [36]. Several experimental studies have exhibited the significance of multi-walled carbon nanotubes (MWCNT) based nanofluids in heat transfer augmentation. The literature also suggests established stability techniques of MWCNTs in oil-based nanosuspensions [37–39]. Carbon nanofibers (CNF) are a new kind of nanomaterials with excellent potential in nanocomposites, tissue engineering, photocatalytic, energy devices, drug delivery, etc. [40–42]. It is generally used as a filler material and relatively inexpensive compared to carbon nanotubes. CNFs are cylindrical-nanostructures with graphene layers arranged irregularly as swirls, cones, or plates. The major difference between CNTs and CNFs is that the graphene layers are perfectly wrapped into a cylindrical structure in the case of CNTs. A few prominent studies [43,44] are found in the literature for CNF-based nanofluids. Zubir et al. [43] measured rheological properties of graphene oxide/water hybrid nanofluids containing CNF, demonstrating a Newtonian phase of hybrid mixture ($< 200\ s^{-1}$) with negligible viscosity change compared to the base fluid (water). Said et al. [44] studied thermo-physical properties of CNF and its hybrid nanofluids with reduced graphene oxide, and concluded that CNF-based nanofluid could be an superlative candidate for high temperature applications .

Recent research trends in nanofluid technology are shifting towards hybrid nanofluids, where the effective thermophysical properties depend on the ratio and loading of two or more nanomaterials. The rheology of hybrid nanofluids is an important characteristic to assess flow behavior. In a recent study [45], it was concluded that a hybrid nanofluid system consisting of spherical and sheet-like nanomaterials attributed to a lower viscosity compared to mono-nanofluid. In another recent study [46], SiO_2 nanosuspensions in mineral oil were experimentally investigated to assess its potential in transformer insulating applications. Nanosuspensions showed variation with shear rate following the power law model and yield stress was observed in all nanofluids. Ma et al. [47] investigated the rheological behavior of Al_2O_3-CuO-water and Al_2O_3-TiO_2-water hybrid nanosuspensions. Nanosuspensions were found stable for 25 days using low

loadings of polyvinyl pyrrolidone (PVP) surfactant. An increase in PVP loading > 0.02 wt% led to a significant increase in viscosity of hybrid nanofluids. Chu et al. [48] examined the rheology of MWCNT-TiO_2 hybrid nanosuspensions in engine oil (5W40). Non-Newtonian and shear thinning behavior was observed at varying temperatures (20-60°C). Said et al. [49] prepared ternary hybrid nanofluid using reduced GO-Fe_3O_4-TiO_2 dispersion in ethylene glycol. A maximum increase of 133.5% was observed for 0.25% loading at 50°C.

There are several experimental studies found on different types of hybrid nanosuspensions. However, investigations on the viscous transport of graphene-based nanofluids in thermal oil are very limited. This research aims to investigate the rheological characteristics of graphene/oil nanofluids and further expand the research by adding MWCNTs and CNFs as hybrid additives. A thorough comparative analysis is provided with an insightful discussion on the impact of hybrid additives on the flow characteristics of graphene/oil nanofluids, and hybrid nanofluids. Three different sets of nanofluids are prepared, consisting of graphene nanoplatelets (G)/thermal oil nanofluids, graphene nanoplatelets - multi-wall carbon nanotubes hybrid (G+CNT)/ thermal oil, and graphene nanoplatelets-carbon nanofiber hybrid (G+CNF)/ thermal oil nanofluids. The methodology is designed to examine the impact of shear forces, temperature, nanomaterial loading, and surfactant loading on the viscosity of three different types of nanofluid sets. A multi-variable correlation is also proposed for the nanofluid viscosity at varying temperatures and nanomaterial loadings.

2. Methodology

2.1 Materials

Three different nanomaterials are utilized in this research. Highly pure graphene nanoplatelets G (Sigma-Aldrich, Malaysia) with 10 nm thickness, <2 μm length, and a specific surface area (SSA) of 750 m^2/g is used. Multi-Walled Carbon Nanotubes (MWCNTs) with a length of 10–20 μm, an inner diameter of 5–12 nm, and an outer diameter of 30-50 nm were acquired from US Research Nanomaterials Inc., (USA). Carbon nanofiber (CNF) of 200 nm average diameter and 20 μm average length was acquired from Carbon Nano (Korea) with a purity of 90%. The details of nanomaterials are compiled in Table 1. The hybrid system of nanomaterials is prepared by adding a similar quantity (1:1 by mass) of both nanomaterials in the base fluid. All acquired nanomaterials are used without any modification.

Table 1: Details from the manufacturer data of the nanomaterials utilized in this investigation.

Nanomaterial	Graphene Nanoplatelets	MWCNTs	CNF
Provenance	Sigma-Aldrich (Malaysia)	US Research Nanomaterials Inc., (USA)	Carbon Nano (Korea)
Purity	> 95%	> 95%	>90%.
Size	10 nm thickness, <2 μm length	5-12 nm (inner diameter), 30-50 nm (outer diameter), 10–20 μm length	200 nm average diameter, 20μm average length
SSA	750m^2/g	> 60 m^2/g	120 m^2/g

A commercial refined thermal oil, Hexatherm (Grade 32) CALTEX, is used as a base fluid. The fluid contains paraffinic content with hydrocarbons ranging from C15 to C50 hydrocarbon and a purity of 70–99 wt%. A non-ionic stabilizer is also utilized to chemically disperse the nanomaterials at varying loadings. Span 85 (sorbitane trioleate) is acquired from Sigma-Aldrich, Malaysia. This stabilizing agent is compatible with oil-based media and has shown excellent stability in the literature [50,51] for several nanofluid combinations.

2.2 Nanomaterial Characterizations

A few characterizations are performed to assess the size, morphology, and chemical composition of mono and hybrid nanomaterials containing graphene, carbon nanotubes, and carbon nanofibers. Five sets of nanomaterial samples are prepared for characterization tests, i.e., graphene nanoplatelets (G), carbon nanotubes (CNT), carbon nanofibers (CNF), graphene + carbon nanotubes hybrid (G+CNT), graphene + carbon nanofibers hybrid (G+CNF), respectively.

Field Emissions Scanning Electron Microscopy FESEM, Zeiss-Supra 55 VP (Germany), and High-Resolution Transmission Electron Microscopy HRTEM, Hitachi HT 7830 UHR (Japan), are used for the morphological characterization. Elemental composition is estimated by Energy Dispersive X-ray spectroscopy EDX Zeiss-Supra 55 VP (Germany). X-ray Diffraction XRD, Bruker D8 (USA), is utilized for structural characterization of mono and hybrid nanomaterials at CuKα radiation $\lambda = 1.54$ A°. The scans are assessed at room temperature over a wide 2θ range of 5-90° with 0.1° step size. Fourier Transform Infrared Reflection FT-IR spectroscopy, Perkin Elmer (USA), is utilized to find the chemical substances and functional groups present in the nanomaterials.

2.3 Preparation of Nanofluids

Three different sets of nanofluids are prepared, consisting of graphene nanoplatelets (G)/thermal oil nanofluids, graphene nanoplatelets - multi-wall carbon nanotubes hybrid (G+CNT)/ thermal oil, and

graphene nanoplatelets – carbon nanofiber hybrid (G+CNF)/ thermal oil nanofluids. A two-step nanofluid preparation method is used to prepare different loadings on nanosuspensions. Equal mass proportions (1:1) of two nanomaterials are used to prepare a hybrid system of nanofluids. In this research, the main reason for choosing equal mass proportion is to explore the possibilities of synergizing effect by the addition of nano-additives and to establish a fundamental knowledge on the behavior of two different nanomaterials in a single system of nanofluid. Based on the outcomes of this fundamental research, future investigations can be further carried out to tune the rheological properties for a specific application by adjusting the mass ratio. The amount of nanomaterial loading in the thermal oil is varied and four different mass loadings are prepared, i.e., 0.5%, 1%, 1.5%, and 2%. Nanofluid's sampling details for the three sets are compiled in Table 2. Two important stability techniques are applied to stabilize nanomaterials in thermal fluid, i.e., ultrasonication and surfactant addition. Both of these techniques have been proven to be an effective dispersion method and de-agglomeration process [52,53]. A probe-type ultrasonicator, Biologics 150V/T (USA), with 20kHz frequency is used to homogenize the nanofluid sample, which is maintained at room temperature during operation using a water-bath. Homogenization is performed at optimized and safe conditions [50,51] for 1 h with 70% power and 30% pulse. The 1-hour sonication process includes the 30% pulse operation, which represents 30% off-duty cycle and 70% on-duty cycle. The chemical stability technique, i.e., surfactant addition is applied by adding an optimized loading of a prominent stabilizer, sorbitane trioleate (Span85), which has excellent properties and nano-oil-based fluid compatibility. This non-ionic stabilizer has non-toxic, anti-corrosion, and non-foaming qualities to a great extent. Span85 is a class of biodegradable surfactants comprising oleic acid-based natural fatty acids and sugar-alcohol sorbitol. It has been applied in several recent studies for the dispersion of nanomaterials in different applications involving emulsion nanofluid membranes [54], Enhanced Oil Recovery (EOR) [55], and other thermofluids [51,56].

To optimize the surfactant loading in the nanofluid samples, several combinations of graphene and hybrid nanofluids are prepared with varying loadings of surfactant. The ultrasonic parameters are remained fixed for all combinations of nanofluids. Visual inspection is performed for at least 30 days to confirm the stability and suitability of the surfactant loading. The optimum nanomaterial to surfactant mass ratio (NP:Span85) in graphene-based nanofluids is found to be 1:3. The optimum NP:Span85 mass ratio for the hybrid G+CNT/ thermal oil nanofluids and hybrid G+CNF/thermal oil nanofluids is set to 1:1 and 1:3, respectively. A large proportion of the surfactant in the nanofluid system can drastically influence the overall thermal behavior of the nanofluid. This manuscript is focused on the rheological profile of the nanofluids. However, the authors intend to extend this research and investigate thermal profile (including the surfactant impact) of the nanofluid in future works.

Table 2: Details of the nanofluid sampling subjected to investigation.

Nanofluid Sets	Set 1 (Mono)	Set 2 (Hybrid)	Set 3 (Hybrid)
Nanomaterial	Graphene nanoplatelets	Graphene nanoplatelets - Multi-wall carbon nanotubes hybrid	Graphene nanoplatelets – carbon nanofiber hybrid
Abbreviation	G	G+CNT Hybrid	G+CNF Hybrid
Nanoadditive mixture ratio (by mass)	-	1:1	1:1
Surfactant to nanomaterial ratio (by mass)	1:3 (optimized)	1:1 (optimized)	1:3 (optimized)
Nanofluid Concentration (mass%)	0.5%, 1%, 1.5%, and 2%	0.5%, 1%, 1.5%, and 2%	0.5%, 1%, 1.5%, and 2%

2.4 Validation of Nanofluids

The nanofluids must be validated prior to measuring thermophysical characteristics or using them in any application. Several tests are performed to validate and justify the applied methodology. These series of tests are performed not only to justify the preparation and stability but also to improve the concept of stability, which is crucial to accurately measure transport properties [57]. First, thermogravimetric analysis (TGA) is performed for thermal oil and Span85 (surfactant) to determine the fluid's thermal stability, as shown in Figure 1(a). The analysis is performed at a constant heat rate and it is found that the degradation of Span 85 stabilizer starts at approximately 600K, whereas, the degradation of thermal oil starts at 500K. This analysis suggests the thermal behavior of Span 85 is better than thermal oil, and it can withstand high temperatures. Figure 1(a) also shows the studied temperature range in this research, i.e., 298 K-338 K for rheology measurements. Hence, proving that the surfactant and the thermal oil will not disintegrate until approximately 500K.

Another thermal stability test is performed on the rheometer, where the viscosity of the three combinations of nanofluids, i.e., G nanofluids, G+CNT hybrid nanofluids, and G+CNF hybrid nanofluids, is measured at 298 K, 318 K and 338 K, illustrated at Figure 1(d-f). The viscosity data points are taken every 31s until the 1200s for the highest loading (2%) of the nanofluids. It is found the change in viscosity values are negligible, and the overall trend is constant with the passage of time. This trend proves that the nanofluids are thermally stable within the studied temperature range. It also proves that the nanofluids did not lose stability at a constant operation/rotation.

In addition, the physical settling test is performed to evaluate the stability of all nanofluid samples using visual inspection at room temperature (301K). Freshly prepared samples are kept at a static condition in batch sedimentation apparatus for thirty days, and the photographs are taken after thirty days of preparation of nanofluid samples to verify the stability. The results are discussed in Section 3.2. Finally, the average particle size distribution of nanofluid samples is obtained using DLS (Dynamic Light Scattering) technique using Zetasizer Nano-S90 (Malvern, UK). The lowest loading (0.5%) of G nanofluid, G+CNT hybrid nanofluid, and G+CNF hybrid nanofluid are analyzed to verify the agglomeration in the samples. The samples are diluted 10 times for DLS analysis because the equipment is not compatible with high loadings of nanosuspensions.

2.5 Rheology measurements and Validation

The rheology of G nanofluids, G+CNT hybrid nanofluids, and G+CNF hybrid nanofluids are experimentally measured using rotational-rheometer, DHR-1 (TA Instruments, US). Rotational-rheometer is initially calibrated with a standard solution of known viscosity. A cone and plate geometry is utilized, as recommended in the literature [58,59]. The specifications of the test cell include steel-made material, Peltier-plate temperature controller system (0.05K), cone angle 2°, truncation gap 55μm, and diameter 60 mm. Proper cleaning is required after every test run, which is also a crucial concern in nanofluid technology [60]. Therefore, a solvent (n-Hexane) is used as a solvent to clean the test cell after every shear ramp operation.

The rheological experiments are performed for four varying loadings of nanomaterial dispersions in thermal oil. A total of twelve samples of nanofluids are utilized for three combinations of Graphene and its hybrid nanofluids and are compared with the rheological behavior of base oil. The rheology of nanofluids and thermal oil is examined at steady shear flow conditions from 1 s^{-1}-2000 s^{-1} at a uniform temperature with a step size of 10 data-points/decade. A similar methodology of shear ramp condition is applied at five different temperatures ranging from 298.15 to 338.15 K (ΔT=10 K) for each sample. Fresh nanofluid samples are prepared with the optimum surfactant loadings. The bubble formations in the sample are avoided. To examine the impact of surfactant on the rheological characteristics, a mixture of oil and Span85 (surfactant) without nanomaterial is subjected to experimental rheology and then compared with the nanofluid (Section 3.6).

The validation of experimental measurement of any device/instrument is crucial to assure the accuracy of the results. The reliability and uncertainty in experimental measurements are considered one of the major concerns in nanofluid technology [61]. The uncertainty analysis of thermal oil at different temperatures is shown in Figure 1(b), exhibiting a declared expanded uncertainty of ±5.5% compared with the literature

[62–67]. The uncertainty in the readings from the measuring instrument is estimated by maximum permissible error (MPE) and the repeatability analysis of the experimental measurements. The consistency of the device is achieved by multiple runs of pure THO as a standard fluid. The combined standard uncertainty and the expanded uncertainty are estimated using coverage factor k=2 (95% confidence). The detailed description of the expanded uncertainty calculations are given in the previous research [51]. The reliability test of the pure base fluid is performed by repeating the experiment thrice at varying temperatures. The temperature profile of thermal oil is shown in Figure 1(c,d). The comparative results show a standard deviation of 0.06%, a relative standard deviation of 2.34%, and an average deviation of 0.04%.

The detailed calculations are available in [51] (using a similar base fluid). Another validation test is performed for the highest loading (2%) of G nanofluid, G+CNT hybrid nanofluid, and G+CNF hybrid nanofluid at three different temperatures, shown in Figure 1(d-f). The shear rate is kept constant at 1000 s^{-1}. The nanofluid is tested for a time-period of 1200 s at a step size of 31 s. The outcomes of Figure 1(d-f) conclude that the nanofluid viscosity at three different temperatures changes minutely and can be considered negligible, hence, exhibiting the efficient performance of the device in handling high loading of nanofluid. It also concludes that the linearity in viscosity represents that the nanofluids are thermally stable in the studied range of temperatures (298 K-338 K). It also endorses that the nanofluids are not subjected to aggregation with time.

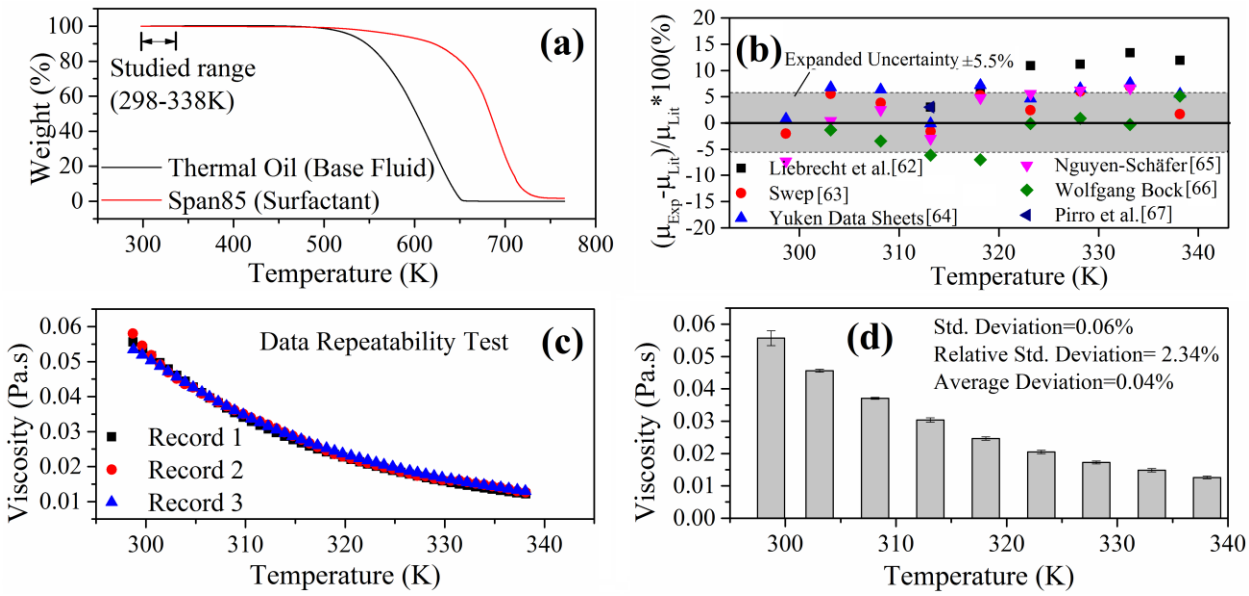

Figure 1: (a) TGA analysis of thermal oil and surfactant; (b) Declared expanded uncertainty and comparisons between literature and experiment for thermal oil [51,62–67]; (c) Repetition of rheology experiments for thermal oil; (d) Representation of viscosity of thermal oil with Y-error bars.

3. Results and Discussion

3.1 Nanomaterial Characterizations

The nanomaterials are subjected to several analytical characterizations prior to preparing nanofluids. Five samples of nanomaterials are prepared for FESEM, HRTEM, EDX, FT-IR, and XRD analysis comprising G, CNT, CNF, G+CNT hybrid (1:1 mixture) and G+CNF hybrid (1:1 mixture). Figure 2 (a-e) and Figure 2(f-j) illustrate the FESEM and TEM micrographs, respectively, to verify the morphology and size of nanomaterials. All nanomaterials in powder form are found in the agglomerated state. Figure 2(a) and 2(f) verify layers of graphene nanoplatelets sheets with thin-layers. The length of the nanoplatelets can be verified, i.e., <2μm. Further details on morphology and size verification are referred to in the previous study [50]. Figures 2(b) and (g) show the tubular structure of multi-walled carbon nanotubes. The outer diameter of nanotubes (30-50nm) and the tube length (10–20μm) can be verified from the micrographs. It is also found that the tubular structures are uniform and the size distribution is consistent. Further morphological details and inner diameter size are evidenced in the previous study [39]. Figure 2(c) and (h) shows the electron microscopy of carbon nanofibers (CNF). Several types of fibrous structures are evident from SEM and TEM analysis. It is also observed that the shape and sizes of nanofibers are not uniform. It not only contains fibrous-structure but also non-uniform tubular or cylindrical structures. The hybrid G+CNT (1:1 mixture) is also subjected to the investigation, and both structures can be seen in one micrograph, shown in Figures 2(d) and (i). A similar trend is also observed for the electron microscopy of G+CNF hybrid (1:1 mixture) nanomaterial, shown in Figures 2(e) and (j). The primary nanometer sizes and morphology of all studied nanomaterials are in agreement with the information provided by the manufacturer.

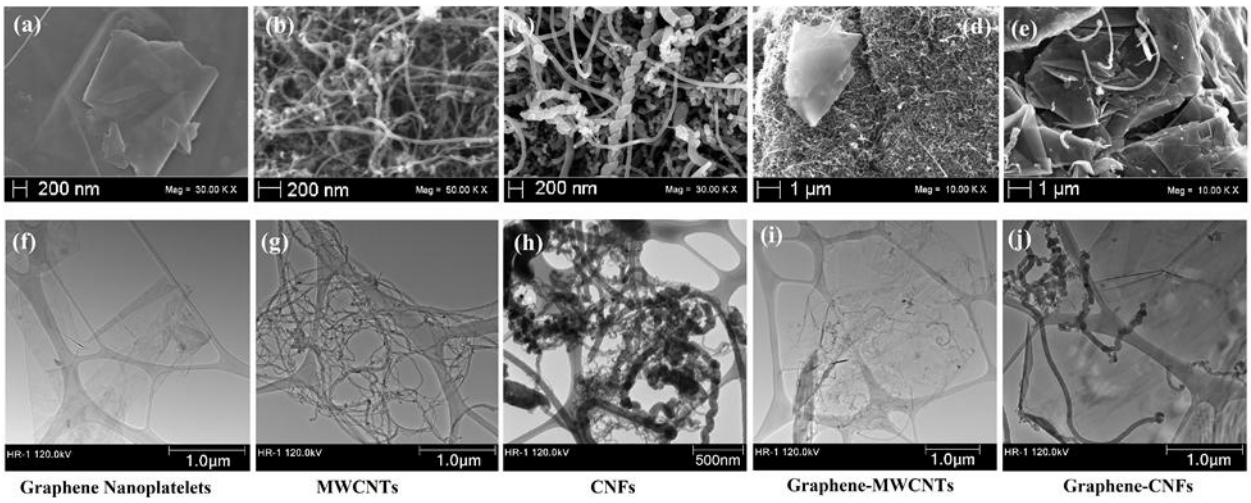

Figure 2: (a-e) FESEM micrographs of the nanomaterials under investigation; (f-j) HRTEM micrographs of nanomaterials under investigation.

The elemental composition of nanomaterials is evaluated using EDX analysis for G, CNT, CNF, G+CNT hybrid (1:1 mixture) and G+CNF hybrid (1:1 mixture), presented in Figure 3(a). The analysis is performed thrice and the average values are presented. All nanomaterials show the presence of pure carbon exceeding 95% by weight. A small amount of oxygen is also found in all samples up to 4%. Trace amounts of containments (Ni, Na, and Fe) are found in a few samples that can be neglected. These contaminents are present either as an impurity or their involvement in nanomaterial fabrication process. The presence of oxygen in the samples is attributed to the exposure of nanomaterial surfaces of nanomaterials in the air since the sample is handled in an open-air system before its utilization in the analytical equipment. Therefore, the nanomaterial surfaces are enriched with oxygen due to chemisorption-induced segregation.

FT-IR scans are performed from 400-4000cm^{-1} for all nanomaterial samples, as shown in Figure 3(b). The major peak in the range of 3000-3500cm^{-1} is referred to as the presence of the -OH stretching functional group due to the humidity in the air [39]. A typical graphite structure peak (C=C) is visible in the range of 1600-1700 cm^{-1} for all nanomaterial samples. The samples with graphene nanomaterials exhibit two more absorption peaks at approximately 1100 cm^{-1} and 1750 cm^{-1}, which is attributed to C=O vibrations [68]. The samples with hybrid nanomaterials do not exhibit any new peak, which assures the non-reactivity and purity of the nanomaterials.

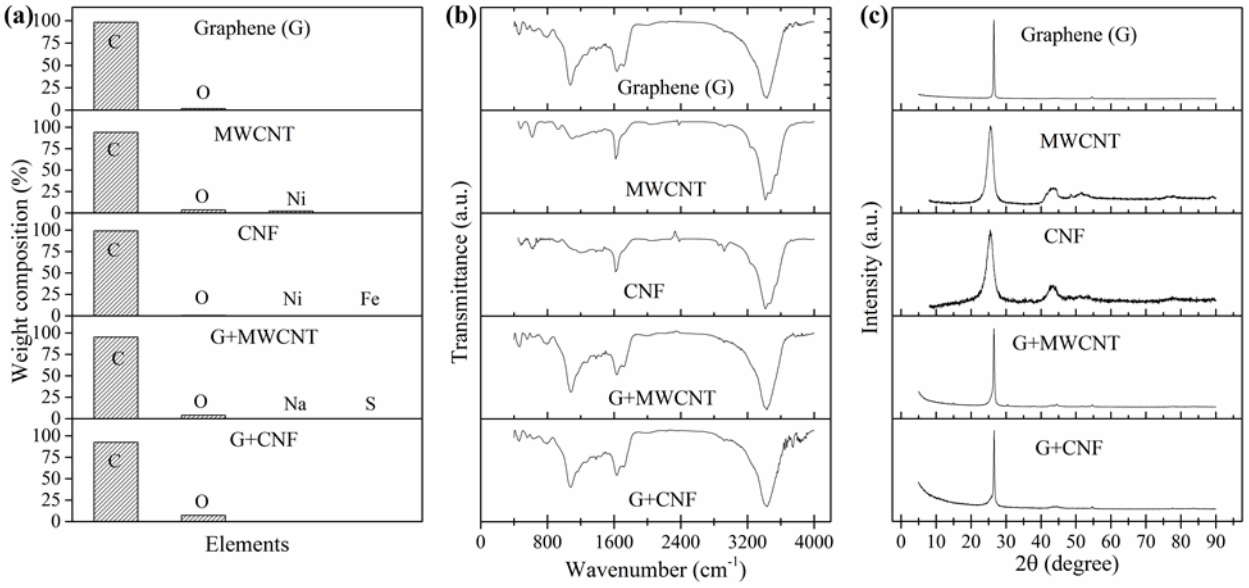

Figure 3: (a) EDX, (b) FT-IR, and (c) XRD analysis of G, CNT, CNF, G+CNT hybrid (1:1 mixture), and G+CNF hybrid (1:1 mixture).

The XRD analysis of G, CNT, CNF, G+CNT hybrid (1:1 mixture) and G+CNF hybrid (1:1 mixture) is performed to examine the crystallographic planes of nanomaterials, shown in Figure 3(c). The diffraction peaks at 2θ=26° and 55° are observed in graphene nanoplatelet samples [69]. The main diffraction peaks in carbon nanotubes and carbon nanofibers at 26°, 43°, 52°, and 77° indicate the presence of carbon-structure [70]. Any new diffraction pattern or band is not visible in the hybrid mixtures, which confirms the purity and quality of the crystallographic structure.

3.2 Stability Evaluation

The stability of nanofluids is often termed the 'validity' of nanofluids. The aggregation among nano-sized materials, due to surface interactions, is the foremost reason for sedimentation at the bottom of the suspension. This phenomenon disturbs the overall fluid flow and transport properties of nanosuspensions. Therefore, the evaluation of stability and the ways to enhance stability must be taken into consideration to validate the nanofluid operation [15]. Ultra-sonication is a significant de-aggregation technique using ultrasonic waves to break nanomaterial agglomerates, that depends on the device type (bath or probe), power, and time of operation [71]. However, the combination of ultra-sonication and surfactant operation has proven long-term stability.

This research involves the evaluation of stability via sedimentation technique and using DLS analysis. It is notable to mention that the stability assessment at rest (static-condition) is a valued-evaluation methodology than the under-flow conditions. All samples of nanosuspensions at varying loadings are subjected to the static condition in glass tubes at room temperatures. The initial sets of samples without surfactant (Span85) exhibited complete sedimentation within three days. Then, fresh samples are prepared with surfactant and ultra-sonication. The ultrasonic parameters and the surfactant loading in the samples are optimized with the objective to reach no-phase separation at resting conditions for at least 30 days. Photographs of all samples are taken after thirty days and compared in Figure 4. Graphene-based nanofluids demonstrate an excellent dispersion for one month using 1:3 (NP:Span85) surfactant loading. The nanomaterial-oil phase separation is not visible in any loading. In the second set of samples (G+CNT hybrid nanofluids), the lowest concertation (0.5%) is starting to exhibit phase separation after thirty days. This set is utilizing 1:1 (NP:Span85) surfactant loading. The amount of surfactant in the hybrid G+CNT nanofluids is relatively low compared to the other two combinations of nanofluids. It is attributed to the fact that MWCNTs can be efficiently stabilized without any surfactant (as proved by a previous study [72]), therefore, the addition of Span 85 is exclusively linked to the presence of graphene nanoplatelets in

the hybrid nanofluids. The third set of hybrid nanofluids involves different loadings of G+CNF hybrid nanofluids, where 1:3 (NP:Span85) surfactant loading is used. All loadings of this set present good stability for thirty days. It is evident from Figure 4 that all G+CNF hybrid nanofluids are starting to lose stability at 30 days demonstrating flocculated-type settling. This behavior of graphene and its hybrid nanofluids undoubtedly recommends that the nanomaterial type play an important role in the stability of nanosuspensions.

DLS analysis is executed on the lowest loading of graphene and its hybrid nanosuspensions. The samples are further diluted 10 times to achieve the particle size distribution results. The analysis is performed within 48 hours of preparation. The results validate the de-aggregation quality of the applied methodology (ultra-sonication and surfactant addition). The average particle sizes are found to be in close proximity to the primary size provided by the manufacturer, and it does not reach a micro-scale agglomerate. The average hydrodynamic particle sizes in G nanofluid, G+CNT hybrid nanofluid, and G+CNF hybrid nanofluid are found to be around 25 nm, 45 nm, and 98 nm, respectively. All nanofluid samples, subjected to DLS analysis, are measured at a fixed scattered angle of 173°.

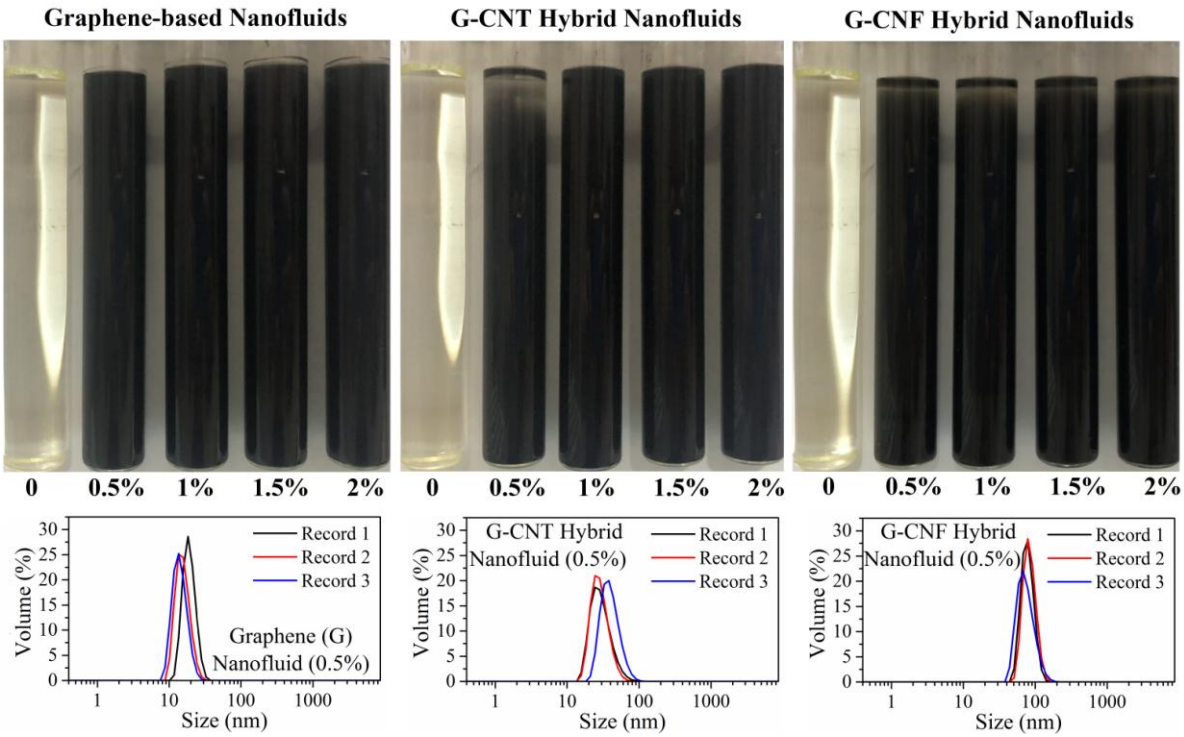

Figure 4: Evaluation of the stability of G nanofluids, G+CNT hybrid nanofluids, and G+CNF hybrid nanofluids using photographs after 30 days and DLS analysis for 0.5% nanofluid loading.

3.3 Flow behavior

Rheological characteristics are assessed by measuring the viscosity of G nanofluids, G+CNT hybrid nanofluids, and G+CNF hybrid nanofluids at varying shear rates. The other variables include temperature and nanomaterial loading. The influence of shear rate on the viscosity of G nanofluids at varying temperatures and loadings is compared in Figure 5. Figure 6 and Figure 7 represent the viscosity vs shear rate trends for G+CNT hybrid nanofluids and G+CNF hybrid nanofluids. All three sets of nanofluids exhibit similar Non-Newtonian flow behavior and can be characterized by the shear-thinning response. The viscosities of thermal oil and all nanofluids at a higher shear rate demonstrate that the fluid may lean towards the Newtonian plateau from the non-Newtonian plateau, but the studied range (1 s^{-1} to 2000 s^{-1}) does not reflect any Newtonian phase. It is evident from Figures 5-7 that the base fluid (thermal oil) exhibits a minimal decline in viscosity over a wide range of shear rates. In comparison, all loadings of nanofluids demonstrate a substantial decline in shear viscosity up to 2000 s^{-1}.

G nanofluids with varying high loadings demonstrate a massive change in the shear-thinning phenomenon compared to low loadings (i.e., 0.5%). The change in shear viscosity of 0.5% loading from 100 s^{-1} to 2000 s^{-1} is negligible, whereas, a slight visible decline in shear viscosity is found at the low shear range (1 s^{-1} to 100 s^{-1}). Interestingly, such a trend is not found in higher loadings of G nanofluids. The higher loadings, i.e., 1%, 1.5% and 2%, shows an immense deterioration in viscosity from 1 s^{-1} to 500 s^{-1} and then, a trivial decline from 500 s^{-1} to 2000 s^{-1}.

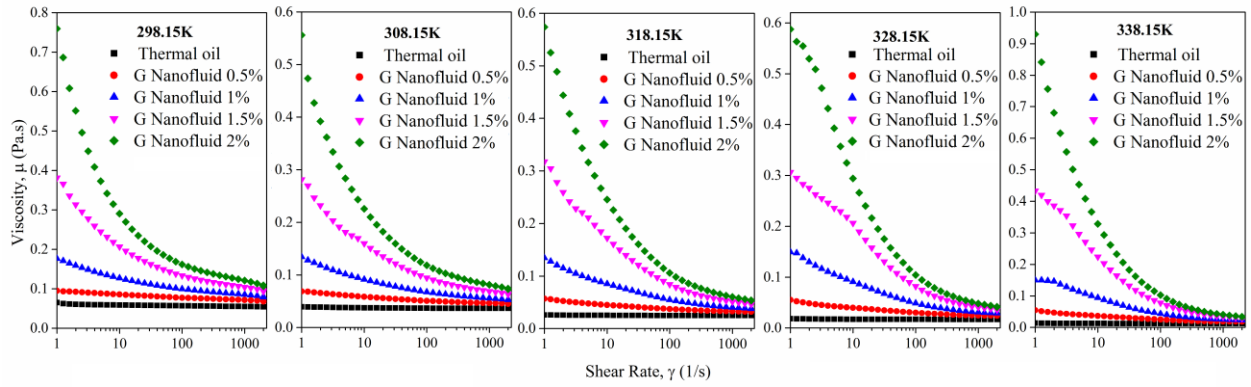

Figure 5: Flow characteristics of thermal oil and G nanofluids at five varying temperatures.

A slightly different trend is observed in Figure 6 for the hybrid system of graphene nanosuspensions containing carbon nanotubes additive. The shear rate ranging from 1 s^{-1} to 50 s^{-1} exhibits a sharp decline in viscosity (steeper decline than G nanofluids). The next phase with a shear rate range of 50 s^{-1} to 2000 s^{-1} exhibits a minimal decline in viscosity. These phenomena are observed similarly for all loadings (0.5%-2%) at five different temperatures. Another important implication from Figure 6 is that the viscosity

values of G-CNT hybrid nanofluids are relatively much higher than G nanofluids in the shear range of 1 s^{-1} to 100 s^{-1}. However, an opposite trend is observed in the shear range of 500 s^{-1} to 2000 s^{-1} (detailed in Section 3.6). These findings suggest that the interactions of different structures, i.e., sheets (graphene) and tubular (CNT), can result in different viscosity trends at a wide shear ramp condition. This analysis also verifies that the shear thinning phenomena can be abolished at higher shear rates using CNTs as an additive in the G nanofluids.

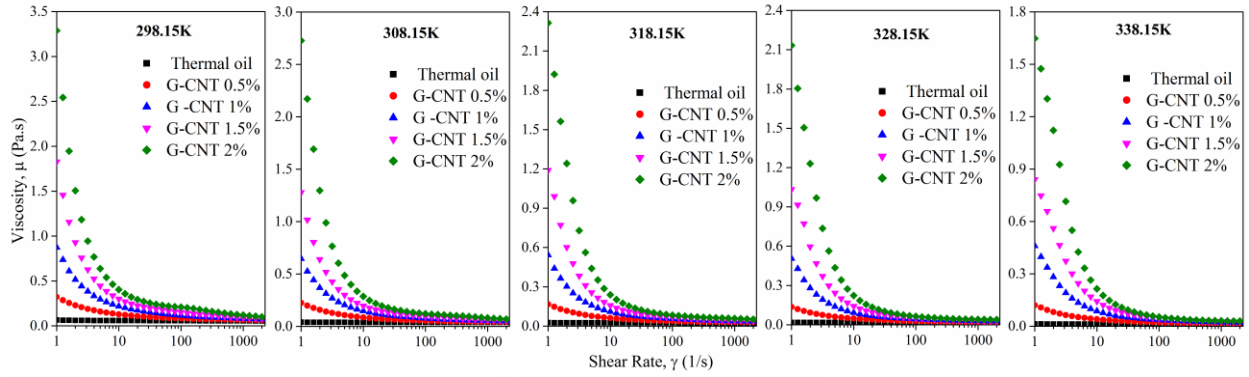

Figure 6: Flow characteristics of thermal oil and G+CNT hybrid nanofluids at five varying temperatures.

The flow behavior trend of nanofluids containing the G+CNF hybrid system is found similar to the G nanofluids at different loadings and temperatures. The flow profile is illustrated in Figure 7. The highest concentration (2%) of G+CNF hybrid nanofluid demonstrates a severe declining viscosity from 1-100 s^{-1}, however, a mild decline is observed from 100-2000 s^{-1}. The profile supports the shear-thinning phenomena from 1 s^{-1} to 2000 s^{-1}, and it is likely to attain Newtonian characteristics at extreme shear rate conditions. The low nanomaterial loadings (0.5%) follow the shear viscosity trend of pure thermal oil.

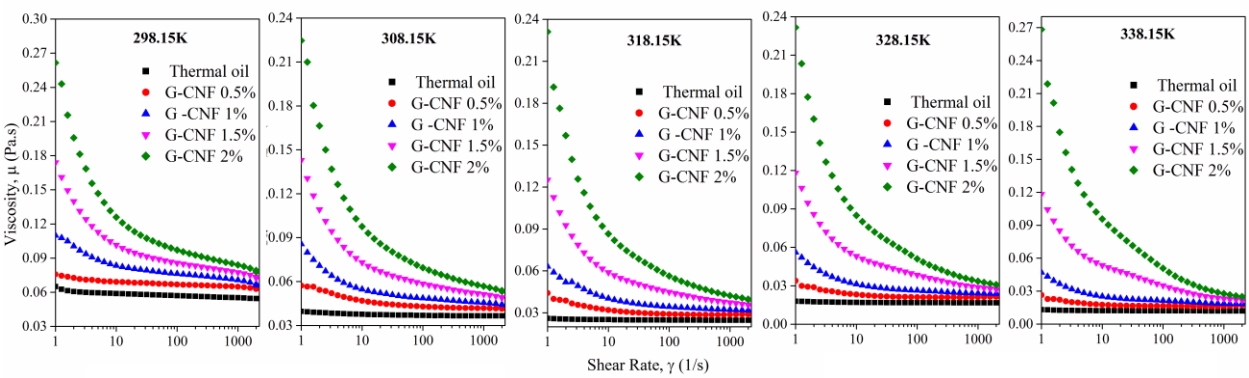

Figure 7: Flow characteristics of thermal oil and G+CNF hybrid nanofluids at five varying temperatures.

The comparison of flow behavior pattern in three types of nanofluid systems (Figure 5-7) reassures that the interaction among different shapes/structures of nanomaterials significantly change the shear viscosity

profile. A similar conclusion was also detailed in the literature [45]. Nanofluids are certainly beneficial for thermal transport, however, the apparent shear viscosity directly affects the pumping power and pressure drop during operation. It may have an adverse impact on the performance of the equipment/device. Therefore, it requires an in-depth investigation of all thermophysical properties of nanofluids. The plausible pressure losses can be moderated by selecting an appropriate flow rate based on the shear-thinning or Newtonian zones in the rheological profile of the nanofluid [73].

The non-Newtonian characteristics are also quantified from shear rate vs shear stress plots at 298 K. The logarithmic plots for G nanofluids, G+CNT hybrid nanofluids, and G+CNF hybrid nanofluids are presented in Figures 8(a), (b), and (c), respectively. Furthermore, the non-Newtonian behavior is quantified using the Power Law model (Ostwald de Waele relationship) and Herschel-Bulkley model (Yield Power Law), given in Eq. 1 and 2, respectively. According to the literature [74], the shear-thinning characteristics of nano-suspensions are often well described by the Power Law model. A similar methodology was also applied by Afrand et al. [75] and Cabaleiro et al. [76].

$$\tau = K\gamma^n \tag{1}$$

$$\tau = \tau_o + K\gamma^n \tag{2}$$

In Eq. 1, the shear stress and shear rate are denoted by τ (Pa) and γ (s^{-1}), respectively. The flow behavior index and flow consistency index are termed as n (-) and k ($Pa{\cdot}s^n$), respectively. The value of n decides the flow behavior type, i.e., $n = 1$ refers to the Newtonian fluid, $n > 1$ refers to shear thickening (non-Newtonian), and $n < 1$ refers to shear thinning (non-Newtonian). Eq. 2 is a modified form of Eq. 1, where a new term is introduced, i.e., yield stress, τ_o (Pa). It is also defined as the resistance to initial flow, where a quantitative amount of stress is required to start the fluid movement. The values of n, k and τ_o are determined using the data fitting technique, and compiled in Figure 9. In this investigation, the Power Law model and Herschel-Bulkley model are applied to all data sets using the curve-fitting technique, and the best fitting model is presented for each data set in Figure 8 based on the lower error matrix.

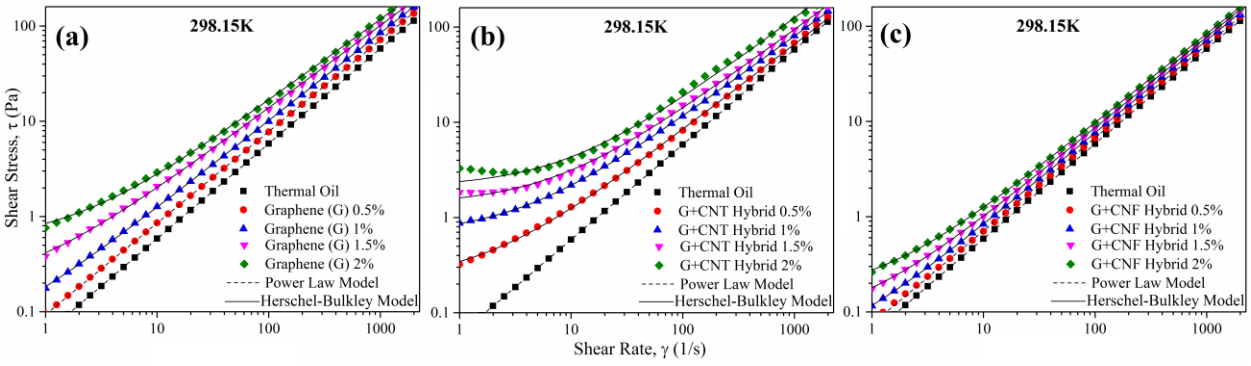

Figure 8: Shear rate vs shear stress behavior of (a) G nanofluids, (b) G+CNT hybrid nanofluids, and (c) G+CNF hybrid nanofluids.

It is evident from Figure 8 that all three sets (G nanofluids, G+CNT hybrid nanofluids, and G+CNF hybrid nanofluids) and thermal oil demonstrate non-Newtonian character. These characteristics can also be assured from the quantification analysis presented in Figure 9(a-c), where the value of the flow index is < 1 in all samples. The flow behavior of thermal oil is in agreement with the Power law model, presented in Figure 8 (dash lines). Similarly, the lowest concentration (0.5%) of G nanofluid and G+CNF hybrid nanofluid exhibit no yield stress ($\tau_o = 0$) and follow the Power Law model, as shown in Figure 8(a,c) and quantified in Figure 9(g, i). All of the other samples follow the Herschel-Bulkley model. An interesting outcome of this analysis shows that the increase in the nanomaterial concentration from 0.5% to 2% attributes to more yield stress. It suggests that the increase in nanomaterial loading constitutes the nanofluids to a high viscosity regime [77], and positive yield stress is required to flow the fluid from a resting position. Sobczak et al. [78] also reported finite yield stress in the shear flow behavior of carbon black nanosuspensions.

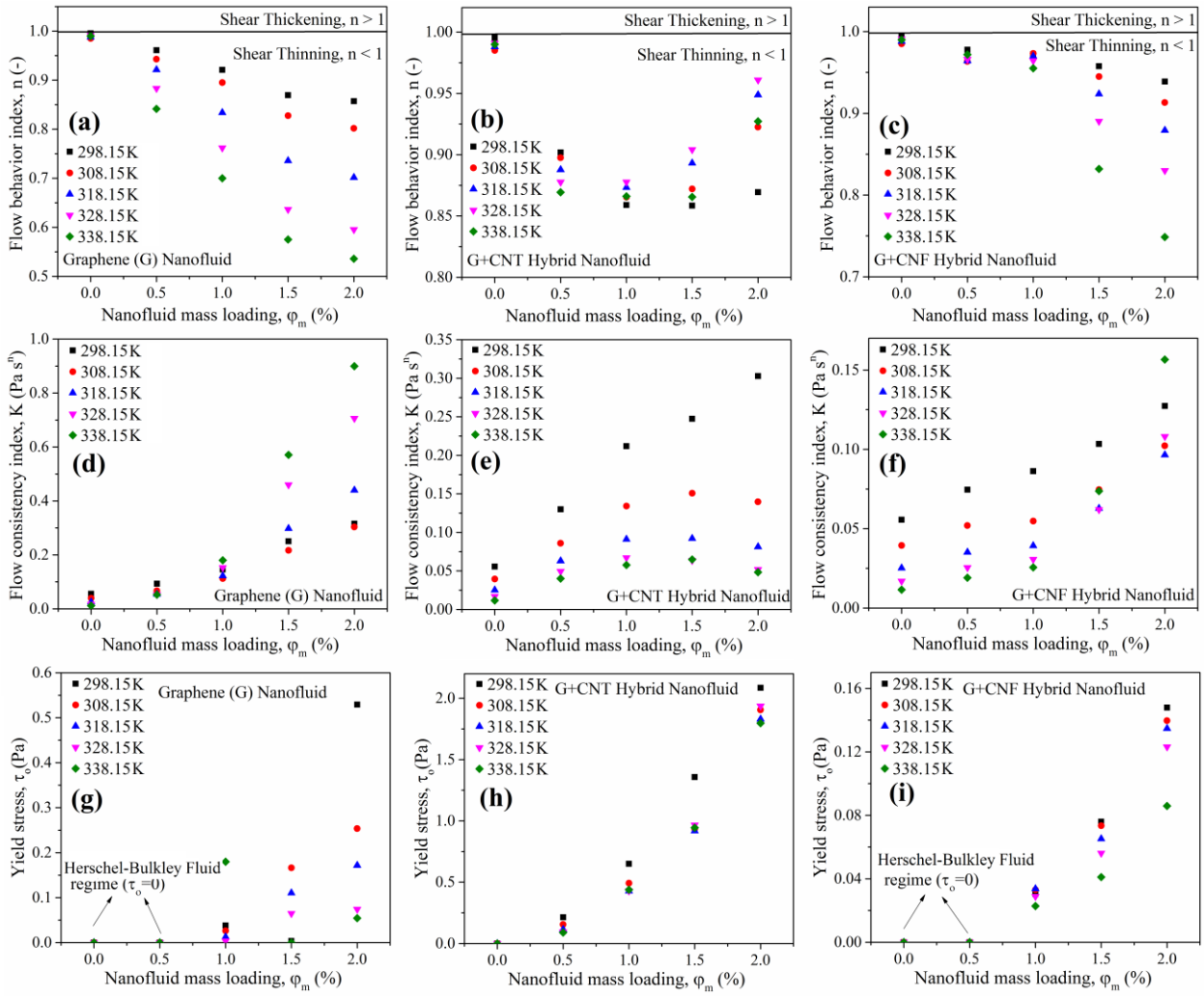

Figure 9: (a-c) Flow behavior index, (d-f) flow consistency index, and (g-i) yield stress of G nanofluids, G+CNT hybrid nanofluids, and G+CNF hybrid nanofluids at varying loadings and temperatures.

Figure 9(a-c) represents the flow behavior index, demonstrating a reduction in the values of n in the case of G nanofluids and G+CNF hybrid nanofluids. It is also found that the higher temperatures correspond to more shear-thinning flow in these samples. However, a different trend is observed in Figure 8(b) for G+CNT hybrid nanofluids, where a curvy-pattern is noticed. The flow index decreases until 1% nanomaterial loading and then increases for 1.5% and 2% loadings. It proposes that the further increase in nanomaterial loadings may tend towards the Newtonian regime or shear-thickening non-Newtonian regime. A similar non-linear pattern is also observed for the flow consistency index in G+CNT hybrid nanofluids, shown in Figure 9(e), whereas, G nanofluids and G+CNF hybrid nanofluids exhibit a similar pattern increasing pattern of k with the increase in nanomaterial loadings. It concludes that the addition of nanotubes as an additive to the graphene-based nanofluids has noteworthy and uncommon results

compared to the carbon nanofiber additives. These outcomes are attributed to the interactions of different structures or shapes of the hybrid nanomaterials, that are corresponding to the unique viscous pattern. Similar justifications for hybrid nanomaterials systems were also detailed by Vallejo et al. [45]. The resulting values of values of n, k and τ_o are totally dependent on the nature and combination of nanomaterials.

3.4 Temperature Dependency

The viscous behavior of G nanofluids, G+CNT hybrid nanofluids, and G+CNF hybrid nanofluids are examined at five different temperatures (298 K-338 K). A comparative analysis of the temperature-velocity relationship at two different shear rates, i.e., 100 s^{-1} and 2000 s^{-1}, is illustrated in Figure 10. Typical decreasing trends in viscosity are observed with the elevation in temperature due to the reduction in binding energy (attractive forces) between the layers of molecules. The mobility of the fluid is increased at high temperatures due to the increase in the thermal and kinetic energy of the molecules.

The percentage viscosity reduction $(\mu_{298K} - \mu_{338K}/\mu_{298K}) \times 100$ for thermal oil from 298 K to 338 K at 100s^{-1} shear rate is calculated to be 79%, whereas, the maximum loading (2%) of G nanofluid, G+CNT hybrid nanofluid, and G+CNF hybrid nanofluid correspond to 36%, 74%, 48%, respectively. At the highest studied shear rate of 2000 s^{-1}, percentage viscosity change for thermal oil, G nanofluid (2%), G+CNT hybrid nanofluid (2%), and G+CNF hybrid nanofluid (2%) constitute a reduction of 78%, 68%, 70%, and 68%, respectively. This analysis confirms that the viscosity reduction with temperature for thermal is appropriately similar for thermal oil at both shear rates. However, the nanofluids reveal a massive change in viscosity reduction at low (100 s^{-1}) and high (2000 s^{-1}) shear rates, where 2% loading of G nanofluid and G+CNF hybrid nanofluid have shown a prominent decrease at high shear rate. The trends in Figure 10 also highlight that the viscosity data points are nearby each other for higher shear rate (2000 s^{-1}) compared to lower shear rate (100 s^{-1}) at varying temperatures. The viscosity reduction for G+CNT hybrid nanofluids at 100 s^{-1} and 2000 s^{-1} are approximately similar. CNT and CNF as an additive to the graphene nanofluids have proved dissimilar results in terms of flow behavior and temperature-viscosity relationship.

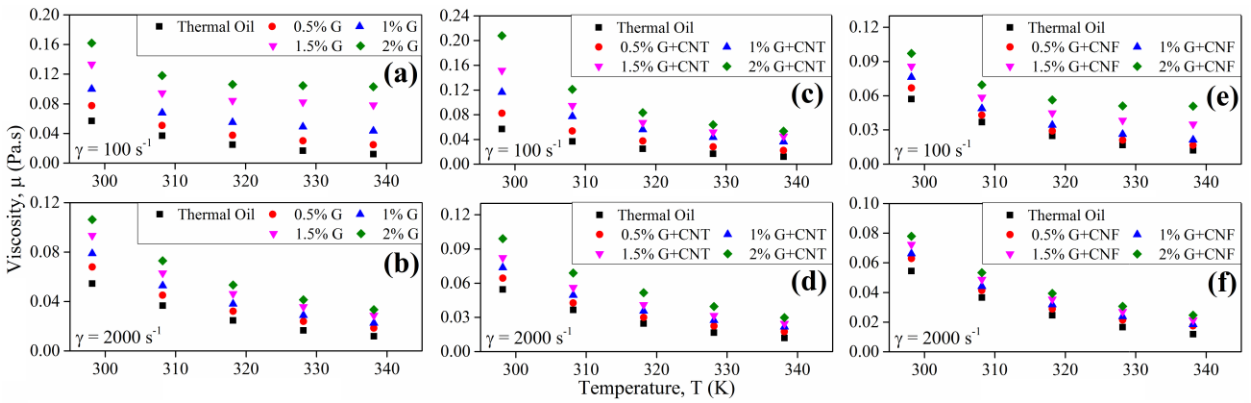

Figure 10: Temperature-viscosity relationship of (a, b) G nanofluids, (c, d) G+CNT hybrid nanofluids, and (e, f) G+CNF hybrid nanofluids at 100 s^{-1} and 2000 s^{-1}.

The literature suggests that VFT (Vogel Fulcher Tammann) model can be utilized to express the viscosity-temperature relationship [45,79,80], given in Eq. 3. Therefore, the data fitting technique is applied, and the fitting parameters μ_o, T_o, and A are compiled in Table 3. The error matrix includes average absolute deviation (AAD) and coefficient of determination (R^2) to assure the performance of the fitting data. The VFT model is found to be in excellent agreement, and the validation is shown in Figure 11. VFT modeling is applied to four different shear rates, i.e., 100 s^{-1}, 500 s^{-1}, 1000 s^{-1}, and 2000 s^{-1}, because the flow curves are not constant and the Newtonian plateau is not observed in any of the studied range (1 s^{-1}-2000 s^{-1}), unlike to the recent investigation by Vallejo et al. [45]. It is noteworthy to indicate that the conventional models (detailed in [21]) are not compared or validated with this experimental research. The literature [61,81] has proved the incompetency of these models because they do not consider temperature, Brownian motion, agglomeration, and other repulsive/attractive forces on phase equilibrium.

$$\mu = \mu_o \times e^{\frac{A}{T-T_o}} \tag{3}$$

Table 3: Fitting parameters of Eq. 3 along with the error matrix for G nanofluids, G+CNT hybrid nanofluids, and G+CNF hybrid nanofluids at varying shear rates.

Shear Rate γ = 100 s^{-1}													
	Oil	Graphene Nanofluids				G+CNT Hybrid Nanofluids				G+CNF Hybrid Nanofluids			
Loading (%)	**0**	**0.5**	**1**	**1.5**	**2**	**0.5**	**1**	**1.5**	**2**	**0.5**	**1**	**1.5**	**2**
μ_o (Pa·s) ×10^{-3}	0.05	7.33	26.84	70.5	94.91	2.19	4.23	10.92	12.31	0.82	1.06	16.76	36.04
A (K)	1000	105.7	31.86	5.37	3.55	259.9	237.9	118.8	119.5	384	383.6	51.63	17.95
T_o (K)	157.5	253.3	273.8	289.7	291.5	226.4	226.3	252.9	255.8	211.1	208.2	266.5	280
AAD (%)	0.22	0.94	0.66	0.64	0.71	0.89	0.77	1.15	0.53	1.38	1.84	1.08	2.05
R^2	0.999	0.999	0.999	0.998	0.997	0.999	0.999	0.999	0.999	0.999	0.999	0.999	0.994
Shear Rate γ = 500 s^{-1}													
	Oil	Graphene Nanofluids				G+CNT Hybrid Nanofluids				G+CNF Hybrid Nanofluids			
Loading (%)	**0**	**0.5**	**1**	**1.5**	**2**	**0.5**	**1**	**1.5**	**2**	**0.5**	**1**	**1.5**	**2**

μ_o (Pa·s) ×10^{-3}	0.05	2.52	4.12	14.5	18.03	1.56	2.32	2.26	0.36	0.82	0.95	2.87	0.29
A (K)	1000	220.9	201.8	84.81	84.49	276.3	275.9	312.8	764.7	384	383.8	246.1	246.1
T_o (K)	157.3	232.6	232.5	256.4	255.4	225.3	222.3	216.8	170.3	211.1	209.6	224	224
AAD (%)	0.37	1.27	0.71	0.72	0.53	1.27	0.42	0.74	1.37	1.38	1.22	1.11	1.11
R^2	0.999	0.999	0.999	0.999	0.999	0.999	0.999	0.999	0.999	0.999	0.999	0.999	0.999
Shear Rate γ = 1000 s^{-1}													
	Oil	Graphene Nanofluids				G+CNT Hybrid Nanofluids				G+CNF Hybrid Nanofluids			
Loading (%)	**0**	**0.5**	**1**	**1.5**	**2**	**0.5**	**1**	**1.5**	**2**	**0.5**	**1**	**1.5**	**2**
μ_o (Pa·s) ×10^{-3}	0.05	1.79	2.47	5.38	6.56	1.57	2.18	1.97	0.67	1.32	1.52	2.08	2.58
A (K)	1000	269.8	269.3	190	189.8	276.3	275.8	323.5	614	290.7	290.5	289.9	289.4
T_o (K)	157.1	224.9	222.1	233.9	233	224.9	221.9	214.4	179.8	223.6	222.5	218.1	214.9
AAD (%)	0.27	1.23	0.74	0.71	0.63	1.38	0.66	1.04	2.17	1.47	0.86	0.67	1.16
R^2	0.999	0.999	0.999	0.999	0.999	0.999	0.999	0.999	0.999	0.999	0.999	0.999	0.999
Shear Rate γ = 2000 s^{-1}													
	Oil	Graphene Nanofluids				G+CNT Hybrid Nanofluids				G+CNF Hybrid Nanofluids			
Loading (%)	**0**	**0.5**	**1**	**1.5**	**2**	**0.5**	**1**	**1.5**	**2**	**0.5**	**1**	**1.5**	**2**
μ_o (Pa·s) ×10^{-3}	0.05	1.93	2.41	3.04	3.67	1.65	2.12	2.5	1.93	1.44	1.64	1.89	2.29
A (K)	1000	259.7	259.4	259.2	259	276	275.6	275.6	382.5	290.4	290.2	290	289.6
T_o (K)	156.4	225.3	223.8	222.4	221.2	223	220.4	219.3	201.1	221.1	219.7	218.6	215.9
AAD (%)	0.398	1.793	1.139	0.803	0.431	1.413	0.448	1.16	1.759	1.15	1.204	0.884	0.886
R^2	0.999	0.999	0.999	0.999	0.999	0.999	0.999	0.999	0.999	0.999	0.999	0.999	0.999

3.5 Nanomaterial Loadings Dependency

Nanomaterial loading is a crucial factor in the realistic design of the nanofluid application. Generally, the loadings contribute to an increase in nanofluid viscosity because these solid particles at the nano-scale provide an additional resistance to flow. Pumping power is generally required in excess for nanofluids compared to base fluids due to high viscosity in the heat transfer operation. The massive increase in viscosity also constitutes unfavorable mechanical performance, as explained by Bakak et al. [82] for G nanofluids.

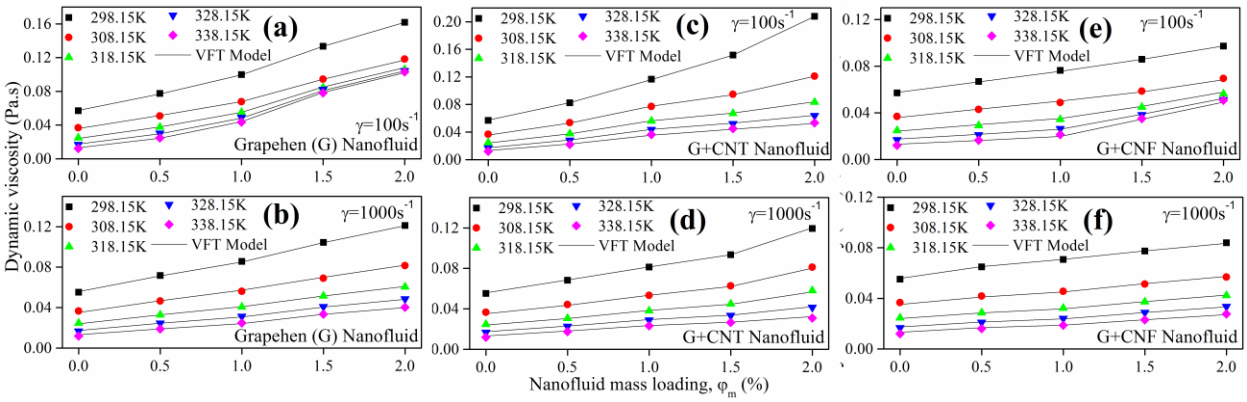

Figure 11: Viscosity-Loading relationship of (a, b) G nanofluids, (c, d) G+CNT hybrid nanofluids, and (e, f) G+CNF hybrid nanofluids at 100 s^{-1} and 1000 s^{-1}, and VFT model comparison.

In this research, the viscosity experiments are performed at four different loadings for G nanofluids, G+CNT hybrid nanofluids, and G+CNF hybrid nanofluids to analyze the nanomaterials' loadings dependency. The main aim of this research is to analyze the impact of CNT and CNF as an additive to G nanofluids because not much literature is available on the comparison of mono-nanofluids with hybrid nanofluids [83]. Typical viscosity-increasing behavior is recognized for all nanofluids at shear rates of 100 s^{-1} and 1000 s^{-1}. The highest viscosity is observed at 2% mass loadings compared to other loadings of G nanofluids, G+CNT hybrid nanofluids, and G+CNF hybrid nanofluids.

The percentage viscosity increment $\left({}^{\mu_{nf}}/_{\mu_{oil}} - 1\right) \times 100$ is evaluated for all three sets of nanofluids at lowest (298 K) and highest temperature (338 K), presented in Figure 12(a-c). The bar graphs represent similar incremental viscosity trends at 100 s^{-1} and 2000 s^{-1} shear rates. The maximum studied temperature, i.e., 338 K, corresponds to a maximum increase in viscosity compared to 298 K for G nanofluids, G+CNT hybrid nanofluids, and G+CNF hybrid nanofluids. The maximum incremental viscosity for G nanofluids is evaluated to be 752% for 2% G loading at 338 K and 100 s^{-1}. This massive increase is attributed to the sheet-type structure of graphene nanoplatelets with huge dimensions of the nanomaterial [50]. At a higher shear rate, i.e., 2000s^{-1}, G nanofluids show a maximum increase of 181%. This suggests that graphene contributes to extreme resistance to shear flow, especially at lower shear rates compared to high shear rates. Therefore, the shear, temperature, and loading profile must be taken into account in the designing of the heat-exchangers or other applications. According to a recent review [84], the highest viscosity enhancement (among the reviewed literature) was reported to be 218% for 0.1% (volumetric) of single-wall CNT dispersions in ethylene glycol at 303K.

One of the major interesting outcomes of this research suggests that the hybrid additives, i.e., CNT and CNF, act as viscosity reducing agents for G nanofluids. Figure 12(b) illustrates that 2% of G+CNT hybrid nanofluids at 338 K exhibits an increment of 340% and 150% at 100 s^{-1} and 2000 s^{-1} shear rates, respectively. Similarly, 2% of G+CNF hybrid nanofluids at 338 K display an augmentation of 319% and 108% at 100 s^{-1} and 2000 s^{-1} shear rates, respectively. Further decrease in effective viscosity of G nanofluid with the addition of CNT or CNF is evaluated by $\left(1 - {}^{\mu_{hybrid}}/_{\mu_{graphene}}\right) \times 100$, shown in Figure 12(d). The analysis demonstrates that the addition of CNT in G nanofluids in equal mass proportions lowers the viscosity of G nanofluids by 12% for 1.5% loading at 298 K and 2000 s^{-1}. Similarly, the addition of CNF in G nanofluids lowers the viscosity by 26% for 2% loading at 298 K and 2000 s^{-1}.

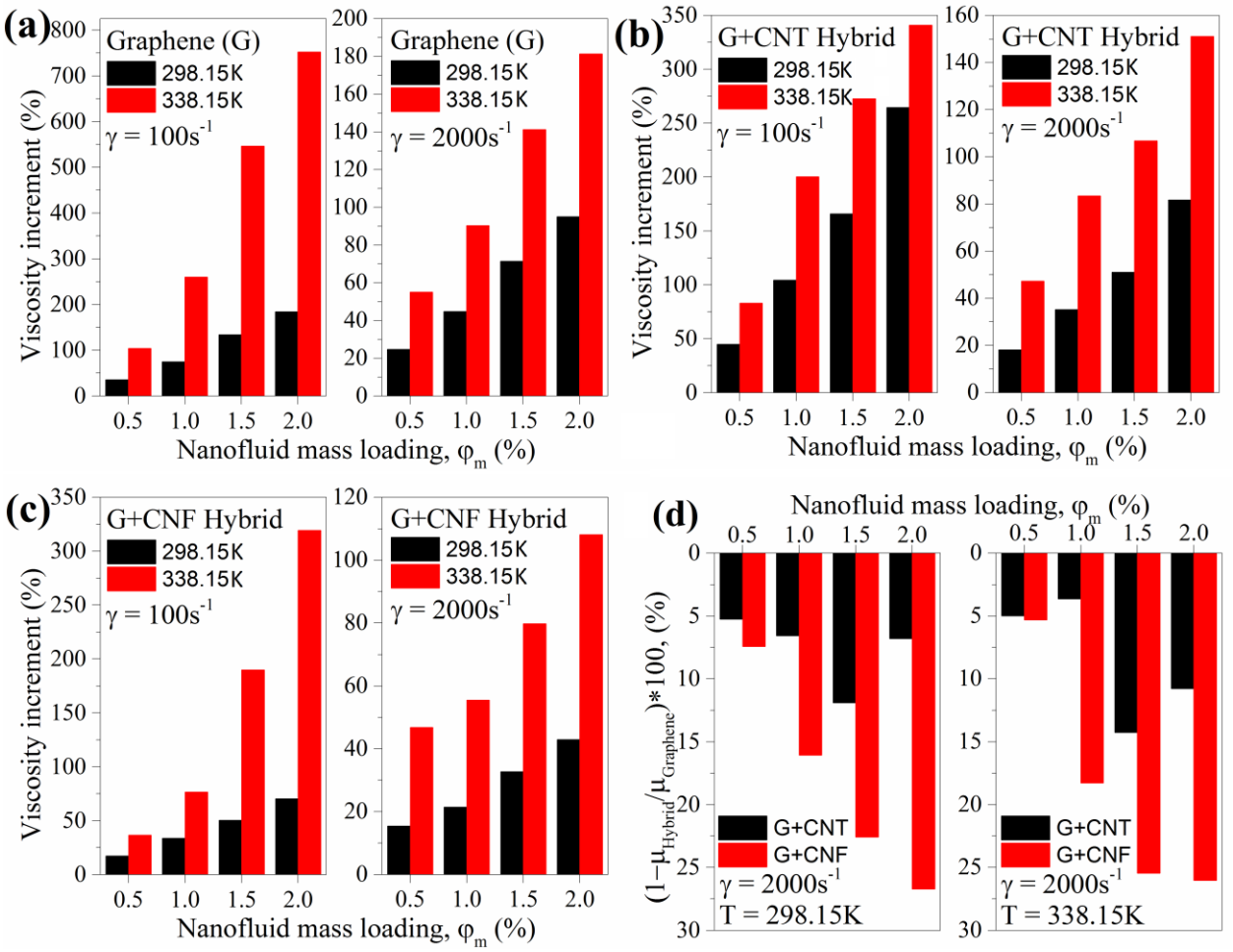

Figure 12: Incremental viscosity of (a) G nanofluids, (b) G+CNT hybrid nanofluids, and (c) G+CNF hybrid nanofluids at varying loadings and temperatures; (d) Decrement in viscosity of G+CNT hybrid nanofluids and G+CNF hybrid with reference to G nanofluids.

It proves that both nanomaterials, CNT and CNF, are able to lower this incremental viscosity of G nanofluids. It is attributed to the interaction of two different structures of G+CNT (nano-sheet + tubular) and G+CNF (nano-sheet + fibrous) that are lowering the effective viscosity of G nanofluids. In another recent study [45], it was concluded that the hybrid system containing sheet-like and spherical particles could lower the viscosity of hybrid nanofluids due to the interactions among them. The entanglement behavior of two different structures due to the high specific surface area can also be correlated with these interesting variations in hybrid nanofluid viscosity [50].

The outcomes of this research are compared with the existing literature using a similar base fluid (thermal oil), shown in Figure 13. Mapping of the viscosity increment with reference to this specific thermal oil is carried out at 298 K temperature and 2000 s^{-1} shear rate for G nanofluids (this study), G+CNT hybrid

nanofluids (this study), and G+CNF hybrid nanofluids (this study), G-Diamond hybrid nanofluids [50], MWCNT nanofluid [72], Diamond nanofluid [51], and functionalized alumina nanofluid [81]. The comparative results reveal that the G nanofluids exhibit incremental viscosity (95% for 2% loading) followed by G-CNT hybrid nanofluids, G-CNF hybrid nanofluid, and G-Diamond nanofluids. It is also found that the viscosity increment of MWCNT nanofluid (0.5% loading) is lower than G-MWCNT hybrid nanofluid, which proves the inclusion of Graphene (G) attributes to the higher viscosity of the hybrid system.

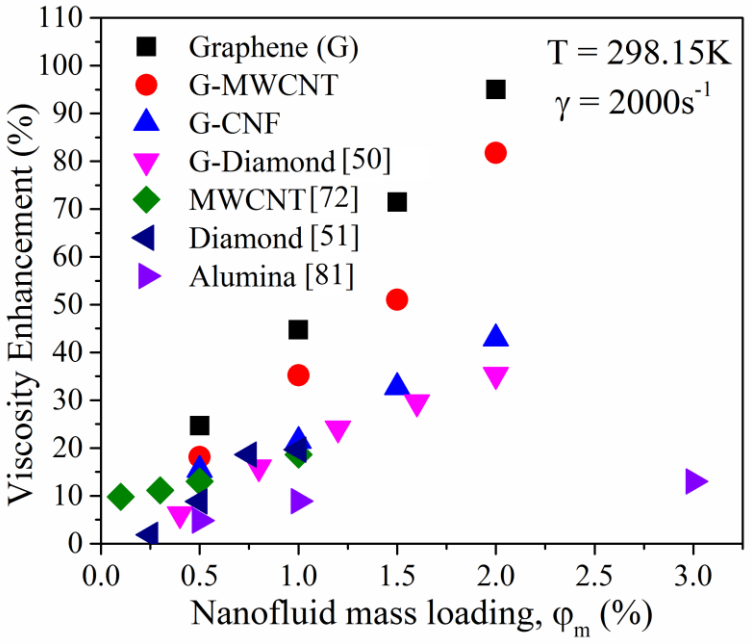

Figure 13: Mapping of viscosity increment with the literature [50,51,72,81].

3.6 Surfactant Loading Dependency

The compatibility of the surfactant is crucial to ingather maximum benefits from nanofluid technology. It includes several factors such as optimum loading, on-foaming qualities, higher degradation temperature, non-reactivity with the nanomaterial, non-toxicity, anti-rusting or anti-scaling agent, and pH controllability. Therefore, special attention must be contributed to the selection of suitable surfactants [85]. The viscosity of surfactant is equally important as a nanofluid, because a minute loading of surfactant may contribute to higher overall viscosity of the nanofluid system and directly impact the pumping power during fluid flow operation [86]. To analyze the sole impact of surfactant on the viscous behavior, nanomaterials (mono or hybrid) are not included in the samples, as shown in Figure 14. However, the amount of surfactant is calculated based on the highest nanomaterial loading of 2%. This

means that the thermal oil+Span85 (1:1) corresponds to thermal oil and surfactant only, and the loading of surfactant is 2% by mass (equivalent to nanomaterial loading 1:1).

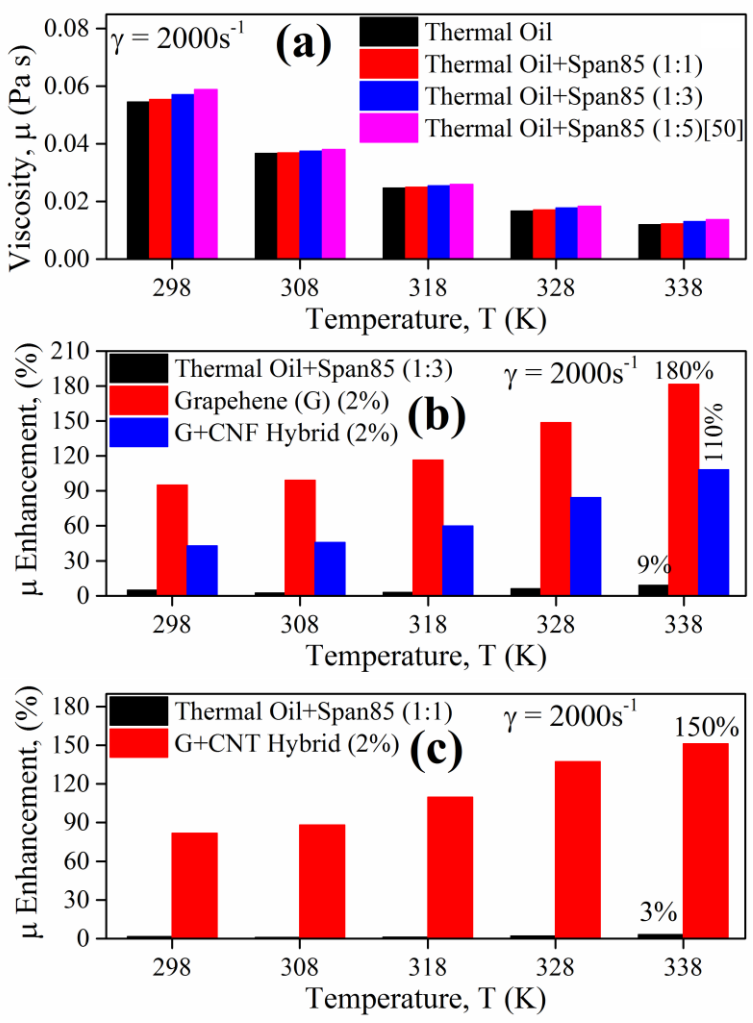

Figure 14: (a) Viscosity comparison of thermal oil and different loadings of surfactant; (b) percentage increment in viscosity of G nanofluid and G+CNF hybrid nanofluid with reference to surfactant (1:3); (c) percentage increment in viscosity of G+CNT hybrid nanofluid with reference to surfactant (1:1).

Figure 14(a) presents a comparison of the viscosity of thermal oil with and without surfactant (Span85). Different loadings of surfactant are compared, and it is found that the addition of Span85 contributes to minute enhancement in overall viscosity. Figure 14(b) represents the comparative analysis of incremental viscosity of base fluid containing thermal oil and Span85 (1:3) with G nanofluid (2%) and G+CNF hybrid nanofluid (2%). This increment is evaluated based on the pure thermal oil as a reference (without surfactant, or any nanomaterial). It is observed that a maximum of 9% viscosity is increased by the addition of Span 85 (1:3) compared to the 180% and 110% increase for G nanofluid and G+CNF hybrid

nanofluid, respectively. Similarly, Figure 14(c) illustrates an increment of 3% only for surfactant (:1) compared to 150% increment for G+CNT hybrid nanofluid (2%). These results suggest that the overall viscosity of the nanofluid system is minutely increased with the increase in Span85 loadings.

3.7 Correlation Development

Vallejo et al. [79,87] proposed a two-variable correlation to predict the viscosity of nanofluids. The correlation consists of nanomaterial loading and temperature, given in Eq. 3. This correlation utilizes volumetric loading, therefore, conversion equations from mass loadings φ_m to volumetric loadings φ_v for G nanofluids and hybrid nanofluids are used [50], given in Eq. 4 and Eq. 5, respectively. True density of nanomaterials are used in Eq. 5, provided by the manufacturer, i.e., 2250 kg/m^3 for graphene nanoplatelets, 2100 kg/m^3 for CNTs, and 1800 kg/m^3 for CNFs. The model is applied to viscosity data of three sets of nanofluids at four different shear rates. In this research, it is found that the viscosity data is not dependent on the last term ($D\varphi_v^2$) of Vallejo model, given in Eq. 3. Therefore, the proposed correlation is reduced to Eq. 6. The fitting parameters of three sets of nanofluids at four shear rate conditions are given in Table 4. The initial term in Eq. 6 can be referred to the base fluid data presented in Table 3. The parity plots are illustrated in Figure 15 for G nanofluids, G+CNT hybrid nanofluids and G+CNF hybrid nanofluids. The predicted data from Eq. 6 lies under ±18% of mean absolute error. In this study, the mean absolute error considering all data points lies under ±18%, where 90% of the data points lies under ±9% mean absolute error.

$$\mu = \mu_o \cdot e^{\frac{A}{T-T_o}} + B\varphi_v \cdot e^{C/T} - D\varphi_v^2 \tag{3}$$

$$\varphi_v = \frac{\varphi_m \times \frac{\rho_{bf}}{\rho_{np}}}{(1-\varphi_m)\times\left(1-\frac{\rho_{bf}}{\rho_{np}}\right)} \tag{4}$$

$$\varphi_v = \left[\frac{0.5\varphi_m \times \frac{\rho_{bf}}{\rho_{np}}}{(1-0.5\varphi_m)\times\left(1-\frac{\rho_{bf}}{\rho_{np}}\right)}\right]_1 + \left[\frac{0.5\varphi_m \times \frac{\rho_{bf}}{\rho_{np}}}{(1-0.5\varphi_m)\times\left(1-\frac{\rho_{bf}}{\rho_{np}}\right)}\right]_2 \tag{5}$$

$$\mu = \mu_o \cdot e^{\frac{A}{T-T_o}} + B\varphi_v \cdot e^{C/T} \tag{6}$$

Table 4: Fitting parameters of Eq. 6 for G nanofluids, G+CNT hybrid nanofluids, and G+CNF hybrid nanofluids at four different shear rates.

Graphene Nanofluids				
Shear rate (s^{-1})	**100**	**500**	**1000**	**2000**
***B* (Pa·s)**	3.14E-02	2.67E-04	5.87E-05	9.21E-07
***C* (K)**	228.05	1585.88	2003.57	3208.63
AAD (%)	8.43	4.14	2.72	6.93
R^2	0.969	0.992	0.996	0.992
G+CNT Hybrid Nanofluids				
Shear rate (s^{-1})	**100**	**500**	**1000**	**2000**
***B* (Pa·s)**	1.76E-06	2.59E-06	8.4E-06	8.93E-05
***C* (K)**	3265.08	2976.16	2535.83	1726.11
AAD (%)	6.15	4.57	3.53	3
R^2	0.982	0.985	0.989	0.993
G+CNF Hybrid Nanofluids				
Shear rate (s^{-1})	**100**	**500**	**1000**	**2000**
***B* (Pa·s) $\times 10^{-7}$**	1.17E-02	0.000578	0.00021	6.00E-04
***C* (K)**	195.47	1016.13	1305.68	925.17
AAD (%)	7.11	2.68	1.81	2.23
R^2	0.981	0.996	0.998	0.997

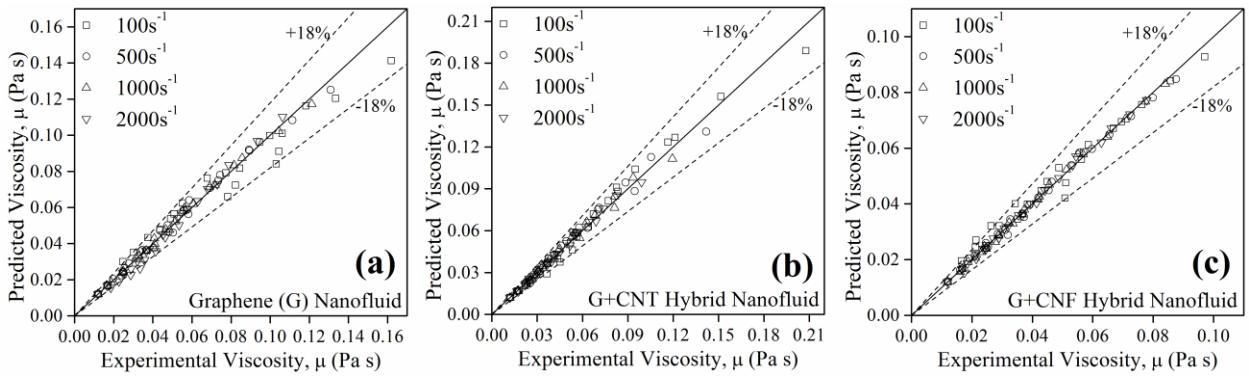

Figure 15: The parity plot of Eq. 6 for (a) G nanofluids, (b) G+CNT hybrid nanofluids, and (c) G+CNF hybrid nanofluids at varying shear rates.

4. Conclusions

This research involves the experimental investigation of the rheological profile of three sets of nanofluids, i.e., G nanofluids, G+CNT hybrid nanofluids, and G+CNF hybrid nanofluids. The morphology of G, CNT, and CNF nanomaterials are validated with several analytical characterizations. Thermofluids are prepared with different loadings using optimum stabilizer and ultrasonication, which proves to be an excellent method to enhance stability for at least one month. The flow behavior affirms the shear-thinning characteristics in all three sets of nanofluids. Thermal oil and low loadings of nanofluids follow the Power Law model, however, an interesting fact is observed when the higher loadings of nanofluids shifted to the Herschel-Bulkley model. Typical declining trends are observed for the viscosity-temperature relationship,

where the VFT model proves to be in excellent agreement with the experimental data. A massive viscosity increase of up to 752%, 340%, and 319% is observed for 2% G nanofluids, G+CNT hybrid nanofluids, and G+CNF hybrid nanofluids, respectively, at 338 K and 100 s^{-1}. However, the increment of viscosity is found lower at higher shear rates. CNT and CNF act as viscosity-reducing additives for G nanofluids and lowers the overall viscosity of G nanofluids by 12% and 26%, respectively. The interactions among two different structures of nanomaterials are one of the major reasons attributed to lowering the viscosity of a hybrid nanofluid system. The addition of Span85 in the nanofluid constitutes a maximum of 9% increase in the overall viscosity of the system. The proposed correlation, based on temperature and nanomaterial loading, shows an excellent agreement with the experimental data.

Authorship Contribution Statement

SU Ilyas: Conceptualization, Methodology, Validation, Formal analysis, Investigation, Writing - Original Draft. **MR Shamsuddin**: Investigation, Methodology, Validation, Resources, Writing - Review & Editing, Project administration, Funding acquisition. **TK Xiang:** Formal analysis, Investigation, Methodology, Validation. **P Estellé:** Conceptualization, Methodology, Validation, Investigation, Writing - Review & Editing. **R Pendyala:** Conceptualization, Methodology, Resources, Writing - Review & Editing, Project administration, Funding acquisition

Declaration of Competing Interests

The authors declare that they have no known competing financial interests or personal relationships that could have appeared to influence the work reported in this paper.

Acknowledgment

This work is supported by the Institute of Autonomous Systems at Universiti Teknologi PETRONAS. The financial assistance is provided by Yayasan UTP (YUTP 015C0-271).

References

[1] A. Banisharif, P. Estellé, A. Rashidi, S. Van Vaerenbergh, M. Aghajani, Heat transfer properties of metal, metal oxides, and carbon water-based nanofluids in the ethanol condensation process, Colloids Surfaces A Physicochem. Eng. Asp. (2021). doi:10.1016/j.colsurfa.2021.126720.

[2] R. Taylor, S. Coulombe, T. Otanicar, P. Phelan, A. Gunawan, W. Lv, G. Rosengarten, R. Prasher, H. Tyagi, Small particles, big impacts: A review of the diverse applications of nanofluids, J. Appl. Phys. 113 (2013) 011301. doi:10.1063/1.4754271.

[3] B. Aghel, S. Janati, F. Alobaid, A. Almoslh, B. Epple, Application of Nanofluids in CO2

Absorption: A Review, Appl. Sci. (2022). doi:10.3390/app12063200.

[4] A.G. Olabi, K. Elsaid, E.T. Sayed, M.S. Mahmoud, T. Wilberforce, R.J. Hassiba, M.A. Abdelkareem, Application of nanofluids for enhanced waste heat recovery: A review, Nano Energy. (2021). doi:10.1016/j.nanoen.2021.105871.

[5] N.A.C. Sidik, T.H. Kean, H.K. Chow, A. Rajaandra, S. Rahman, J. Kaur, Performance enhancement of cold thermal energy storage system using nanofluid phase change materials: A review, Int. Commun. Heat Mass Transf. (2018). doi:10.1016/j.icheatmasstransfer.2018.03.024.

[6] G. Nobrega, R.R. de Souza, I.M. Gonçalves, A.S. Moita, J.E. Ribeiro, R.A. Lima, Recent Developments on the Thermal Properties, Stability and Applications of Nanofluids in Machining, Solar Energy and Biomedicine, Appl. Sci. (2022). doi:10.3390/app12031115.

[7] R.R. Souza, I.M. Gonçalves, R.O. Rodrigues, G. Minas, J.M. Miranda, A.L.N. Moreira, R. Lima, G. Coutinho, J.E. Pereira, A.S. Moita, Recent advances on the thermal properties and applications of nanofluids: From nanomedicine to renewable energies, Appl. Therm. Eng. (2022). doi:10.1016/j.applthermaleng.2021.117725.

[8] M. Pavía, K. Alajami, P. Estellé, A. Desforges, B. Vigolo, A critical review on thermal conductivity enhancement of graphene-based nanofluids, Adv. Colloid Interface Sci. (2021). doi:10.1016/j.cis.2021.102452.

[9] A.H. Arain, S. Ridha, S.U. Ilyas, M.E. Mohyaldinn, R.R. Suppiah, Evaluating the influence of graphene nanoplatelets on the performance of invert emulsion drilling fluid in high-temperature wells, J. Pet. Explor. Prod. Technol. (2022) 1–25. doi:10.1007/s13202-022-01501-5.

[10] N.A.C. Sidik, H.A. Mohammed, O.A. Alawi, S. Samion, A review on preparation methods and challenges of nanofluids, Int. Commun. Heat Mass Transf. 54 (2014) 115–125. doi:10.1016/j.icheatmasstransfer.2014.03.002.

[11] M.H. Ahmadi, A. Mirlohi, M. Alhuyi Nazari, R. Ghasempour, A review of thermal conductivity of various nanofluids, J. Mol. Liq. (2018). doi:10.1016/j.molliq.2018.05.124.

[12] H. Babar, H.M. Ali, Towards hybrid nanofluids: Preparation, thermophysical properties, applications, and challenges, J. Mol. Liq. (2019). doi:10.1016/j.molliq.2019.02.102.

[13] M. Muneeshwaran, G. Srinivasan, P. Muthukumar, C.C. Wang, Role of hybrid-nanofluid in heat transfer enhancement – A review, Int. Commun. Heat Mass Transf. (2021). doi:10.1016/j.icheatmasstransfer.2021.105341.

[14] Z. Xuan, Y. Zhai, M. Ma, Y. Li, H. Wang, Thermo-economic performance and sensitivity analysis of ternary hybrid nanofluids, J. Mol. Liq. (2021). doi:10.1016/j.molliq.2020.114889.

[15] S.U. Ilyas, R. Pendyala, N. Marneni, Stability of Nanofluids, Eng. Appl. Nanotechnol. (2017) 1–31. doi:10.1007/978-3-319-29761-3_1.

[16] S. Chakraborty, P.K. Panigrahi, Stability of nanofluid: A review, Appl. Therm. Eng. 174 (2020) 115259. doi:10.1016/j.applthermaleng.2020.115259.

[17] K. Cacua, F. Ordoñez, C. Zapata, B. Herrera, E. Pabón, R. Buitrago-Sierra, Surfactant concentration and pH effects on the zeta potential values of alumina nanofluids to inspect stability, Colloids Surfaces A Physicochem. Eng. Asp. (2019). doi:10.1016/j.colsurfa.2019.123960.

[18] A. Gallego, K. Cacua, B. Herrera, D. Cabaleiro, M.M. Piñeiro, L. Lugo, Experimental evaluation of the effect in the stability and thermophysical properties of water-Al2O3 based nanofluids using SDBS as dispersant agent, Adv. Powder Technol. 31 (2020) 560–570. doi:10.1016/j.apt.2019.11.012.

[19] N.A. Che Sidik, M. Mahmud Jamil, W.M.A. Aziz Japar, I. Muhammad Adamu, A review on preparation methods, stability and applications of hybrid nanofluids, Renew. Sustain. Energy Rev. 80 (2017) 1112–1122. doi:10.1016/j.rser.2017.05.221.

[20] S.N. Suhaimi, A.R.A. Rahman, M.F.M. Din, M.Z. Hassan, M.T. Ishak, M.T. Bin Jusoh, A Review on Oil-Based Nanofluid as Next-Generation Insulation for Transformer Application, J. Nanomater. (2020). doi:10.1155/2020/2061343.

[21] A. Asadi, S. Aberoumand, A. Moradikazerouni, F. Pourfattah, G. Żyła, P. Estellé, O. Mahian, S. Wongwises, H.M. Nguyen, A. Arabkoohsar, Recent advances in preparation methods and thermophysical properties of oil-based nanofluids: A state-of-the-art review, Powder Technol. 352 (2019) 209–226. doi:10.1016/j.powtec.2019.04.054.

[22] S.M.S. Murshed, P. Estellé, A state of the art review on viscosity of nanofluids, Renew. Sustain. Energy Rev. 76 (2017) 1134–1152. doi:10.1016/j.rser.2017.03.113.

[23] S.M. Sohel Murshed, P. Estellé, Rheological characteristics of nanofluids for advance heat transfer, in: Adv. New Heat Transf. Fluids From Numer. to Exp. Tech., 2017. doi:10.1201/9781315368184.

[24] S.R. Yan, D. Toghraie, L.A. Abdulkareem, A. Alizadeh, P. Barnoon, M. Afrand, The rheological behavior of MWCNTs–ZnO/Water–Ethylene glycol hybrid non-Newtonian nanofluid by using of

an experimental investigation, J. Mater. Res. Technol. (2020). doi:10.1016/j.jmrt.2020.05.018.

[25] G. Colangelo, E. Favale, P. Miglietta, M. Milanese, A. de Risi, Thermal conductivity, viscosity and stability of Al2O3-diathermic oil nanofluids for solar energy systems, Energy. (2016). doi:10.1016/j.energy.2015.11.032.

[26] A. Asadi, M. Asadi, A. Rezaniakolaei, L.A. Rosendahl, M. Afrand, S. Wongwises, Heat transfer efficiency of Al2O3-MWCNT/thermal oil hybrid nanofluid as a cooling fluid in thermal and energy management applications: An experimental and theoretical investigation, Int. J. Heat Mass Transf. (2018). doi:10.1016/j.ijheatmasstransfer.2017.10.036.

[27] E. Dardan, M. Afrand, A.H. Meghdadi Isfahani, Effect of suspending hybrid nano-additives on rheological behavior of engine oil and pumping power, Appl. Therm. Eng. (2016). doi:10.1016/j.applthermaleng.2016.08.103.

[28] M. Fakoor Pakdaman, M.A. Akhavan-Behabadi, P. Razi, An experimental investigation on thermo-physical properties and overall performance of MWCNT/heat transfer oil nanofluid flow inside vertical helically coiled tubes, Exp. Therm. Fluid Sci. (2012). doi:10.1016/j.expthermflusci.2012.02.005.

[29] X. Li, C. Zou, L. Zhou, A. Qi, Experimental study on the thermo-physical properties of diathermic oil based SiC nanofluids for high temperature applications, Int. J. Heat Mass Transf. (2016). doi:10.1016/j.ijheatmasstransfer.2016.02.056.

[30] A.G. Olabi, M.A. Abdelkareem, T. Wilberforce, E.T. Sayed, Application of graphene in energy storage device – A review, Renew. Sustain. Energy Rev. (2021). doi:10.1016/j.rser.2020.110026.

[31] S.K. Tiwari, S. Sahoo, N. Wang, A. Huczko, Graphene research and their outputs: Status and prospect, J. Sci. Adv. Mater. Devices. (2020). doi:10.1016/j.jsamd.2020.01.006.

[32] Y. Yan, W.I. Shin, H. Chen, S.M. Lee, S. Manickam, S. Hanson, H. Zhao, E. Lester, T. Wu, C.H. Pang, A recent trend: application of graphene in catalysis, Carbon Lett. (2021). doi:10.1007/s42823-020-00200-7.

[33] S. Hamze, N. Berrada, D. Cabaleiro, A. Desforges, J. Ghanbaja, J. Gleize, D. Bégin, F. Michaux, T. Maré, B. Vigolo, P. Estellé, Few-layer graphene-based nanofluids with enhanced thermal conductivity, Nanomaterials. (2020). doi:10.3390/nano10071258.

[34] X. Hou, Y. Ma, G. Bhandari, Z. Yin, L. Dai, H. Liao, Y. Wei, Preparation and tribological properties of graphene lubricant additives for low-sulfur fuel by dielectric barrier discharge

plasma-assisted ball milling, Processes. (2021). doi:10.3390/pr9020272.

[35] J. Zhao, T. Gao, Y. Li, Y. He, Y. Shi, Two-dimensional (2D) graphene nanosheets as advanced lubricant additives: A critical review and prospect, Mater. Today Commun. (2021). doi:10.1016/j.mtcomm.2021.102755.

[36] R. Vetrivel, C. Navinselvakumar, P.S. Samuel Ratna Kumar, Carbon nanotubes and its applications – A review, Int. J. Mech. Prod. Eng. Res. Dev. (2018).

[37] P. Yadav, S.M. Gupta, S.K. Sharma, A review on stabilization of carbon nanotube nanofluid, J. Therm. Anal. Calorim. (2022). doi:10.1007/s10973-021-10999-6.

[38] A. Nasiri, M. Shariaty-Niasar, A. Rashidi, A. Amrollahi, R. Khodafarin, Effect of dispersion method on thermal conductivity and stability of nanofluid, Exp. Therm. Fluid Sci. (2011). doi:10.1016/j.expthermflusci.2011.01.006.

[39] S.U. Ilyas, R. Pendyala, M. Narahari, Stability and thermal analysis of MWCNT-thermal oil-based nanofluids, Colloids Surfaces A Physicochem. Eng. Asp. 527 (2017) 11–22. doi:10.1016/j.colsurfa.2017.05.004.

[40] Z. Wang, S. Wu, J. Wang, A. Yu, G. Wei, Carbon nanofiber-based functional nanomaterials for sensor applications, Nanomaterials. (2019). doi:10.3390/nano9071045.

[41] Trabelsi, Mamun, Klöcker, Sabantina, Großerhode, Blachowicz, Ehrmann, Increased Mechanical Properties of Carbon Nanofiber Mats for Possible Medical Applications, Fibers. (2019). doi:10.3390/fib7110098.

[42] Kenry, C.T. Lim, Nanofiber technology: current status and emerging developments, Prog. Polym. Sci. (2017). doi:10.1016/j.progpolymsci.2017.03.002.

[43] M.N. Mohd Zubir, A. Badarudin, S.N. Kazi, H. Nay Ming, R. Sadri, A. Amiri, Investigation on the Use of Graphene Oxide as Novel Surfactant for Stabilizing Carbon Based Materials, J. Dispers. Sci. Technol. (2016). doi:10.1080/01932691.2015.1108850.

[44] Z. Said, M.A. Abdelkareem, H. Rezk, A.M. Nassef, H.Z. Atwany, Stability, thermophysical and electrical properties of synthesized carbon nanofiber and reduced-graphene oxide-based nanofluids and their hybrid along with fuzzy modeling approach, Powder Technol. (2020). doi:10.1016/j.powtec.2020.02.026.

[45] J.P. Vallejo, G. Żyła, L. Ansia, J. Fal, J. Traciak, L. Lugo, Thermophysical, rheological and

electrical properties of mono and hybrid TiB2/B4C nanofluids based on a propylene glycol:water mixture, Powder Technol. (2022). doi:10.1016/j.powtec.2021.09.074.

[46] S.K. Amizhtan, A.J. Amalanathan, M.S. Babu, R. Sarathi, G. Kumar, J.S. Sangwai, H. Edin, N. Taylor, Experimental Study and ANN Analysis of Rheological Behavior of Mineral Oil-based SiO2 Nanofluids, IEEE Trans. Dielectr. Electr. Insul. (2022) 1–1. doi:10.1109/TDEI.2022.3173514.

[47] M. Ma, Y. Zhai, P. Yao, Y. Li, H. Wang, Effect of surfactant on the rheological behavior and thermophysical properties of hybrid nanofluids, Powder Technol. (2021). doi:10.1016/j.powtec.2020.10.089.

[48] Y.M. Chu, M. Ibrahim, T. Saeed, A.S. Berrouk, E.A. Algehyne, R. Kalbasi, Examining rheological behavior of MWCNT-TiO2/5W40 hybrid nanofluid based on experiments and RSM/ANN modeling, J. Mol. Liq. (2021). doi:10.1016/j.molliq.2021.115969.

[49] Z. Said, N.K. Cakmak, P. Sharma, L.S. Sundar, A. Inayat, O. Keklikcioglu, C. Li, Synthesis, stability, density, viscosity of ethylene glycol-based ternary hybrid nanofluids: Experimental investigations and model -prediction using modern machine learning techniques, Powder Technol. (2022). doi:10.1016/j.powtec.2022.117190.

[50] S.U. Ilyas, S. Ridha, S. Sardar, P. Estellé, A. Kumar, R. Pendyala, Rheological behavior of stabilized diamond-graphene nanoplatelets hybrid nanosuspensions in mineral oil, J. Mol. Liq. 328 (2021). doi:10.1016/j.molliq.2021.115509.

[51] S.U. Ilyas, M. Narahari, R. Pendyala, Rheological characteristics of ultrastable diamond-thermal oil nanofluids, J. Mol. Liq. (2020). doi:10.1016/j.molliq.2020.113098.

[52] H.S. Shamsuddin, P. Estellé, J. Navas, N. Mohd-Ghazali, M. Mohamad, Effects of surfactant and nanofluid on the performance and optimization of a microchannel heat sink, Int. J. Heat Mass Transf. (2021). doi:10.1016/j.ijheatmasstransfer.2021.121336.

[53] A. Afzal, I. Nawfal, I.M. Mahbubul, S.S. Kumbar, An overview on the effect of ultrasonication duration on different properties of nanofluids, J. Therm. Anal. Calorim. (2019). doi:10.1007/s10973-018-7144-8.

[54] H.P. Kohli, S. Gupta, M. Chakraborty, Stability and performance study of emulsion nanofluid membrane: A combined approach of adsorption and extraction of Ethylparaben, Colloids Surfaces A Physicochem. Eng. Asp. (2019). doi:10.1016/j.colsurfa.2019.123675.

[55] A. Karimi, Z. Fakhroueian, A. Bahramian, N. Pour Khiabani, J.B. Darabad, R. Azin, S. Arya, Wettability alteration in carbonates using zirconium oxide nanofluids: EOR implications, Energy and Fuels. (2012). doi:10.1021/ef201475u.

[56] I. Javed, S.W. Baek, K. Waheed, Evaporation characteristics of heptane droplets with the addition of aluminum nanoparticles at elevated temperatures, Combust. Flame. (2013). doi:10.1016/j.combustflame.2012.09.005.

[57] S. Hamze, D. Cabaleiro, P. Estellé, Graphene-based nanofluids: A comprehensive review about rheological behavior and dynamic viscosity, J. Mol. Liq. (2021). doi:10.1016/j.molliq.2020.115207.

[58] B. Muñoz-Sánchez, J. Nieto-Maestre, E. Veca, R. Liberatore, S. Sau, H. Navarro, Y. Ding, N. Navarrete, J.E. Juliá, Á.G. Fernández, A. García-Romero, Rheology of Solar-Salt based nanofluids for concentrated solar power. Influence of the salt purity, nanoparticle concentration, temperature and rheometer geometry, Sol. Energy Mater. Sol. Cells. (2018). doi:10.1016/j.solmat.2017.10.022.

[59] E. Sani, J.P. Vallejo, D. Cabaleiro, L. Lugo, Functionalized graphene nanoplatelet-nanofluids for solar thermal collectors, Sol. Energy Mater. Sol. Cells. (2018). doi:10.1016/j.solmat.2018.05.038.

[60] N. COST Action CA, 15119, Report about nanofluid's health, safety and environmental impact, 2019. doi:10.6035/ca15119.2019.02.

[61] Nanouptake Cost Action CA 15119, Report about industrial perspectives on nanofluids market uptake, Castello de la Plana (Spain), 2019. doi:10.6035/CA15119.2019.01.

[62] J. Liebrecht, X. Si, B. Sauer, H. Schwarze, Investigation of drag and churning losses on tapered roller bearings, Stroj. Vestnik/Journal Mech. Eng. 61 (2015) 399–408. doi:10.5545/sv-jme.2015.2490.

[63] Swep, Industrial handbook introudction - oil as a heat transfer fluid, (n.d.). doi:https://www.swep.net/industrial-handbook/industrial-handbook/.

[64] Yukun Engineering Standards, Data Sheets: Formulas/Nomograms (Part 4) Viscosity Vs. Temperature Charts, n.d.

[65] H. Nguyen-Schäfer, Applied tribology in the oil-film bearings, in: Springer Tracts Mech. Eng., 2015. doi:10.1007/978-3-319-17644-4_9.

[66] Encyclopedia of Lubricants and Lubrication, 2014. doi:10.1007/978-3-642-22647-2.

[67] J.-B. Wu, M.-L. Lin, X. Cong, H.-N. Liu, P.-H. Tan, Raman spectroscopy of graphene-based materials and its applications in related devices, Chem. Soc. Rev. 47 (2018) 1822–1873. doi:10.1039/C6CS00915H.

[68] C. Zapata-Hernandez, G. Durango-Giraldo, D. López, R. Buitrago-Sierra, K. Cacua, Surfactants versus surface functionalization to improve the stability of graphene nanofluids, J. Dispers. Sci. Technol. (2021). doi:10.1080/01932691.2021.1880429.

[69] V.Q. Tran, H.T. Doan, N.T. Nguyen, C. V. Do, A.K. Sharma, Preparation of graphene nanoplatelets by thermal shock combined with ball milling methods for fabricating flame-retardant polymers, J. Chem. (2019). doi:10.1155/2019/5284160.

[70] M. Sharon, M. Sharon, Effect of Inherent Anatomy of Plant Fibers on the Morphology of Carbon Synthesized from Them and Their Hydrogen Absorption Capacity, Carbon Lett. (2012). doi:10.5714/cl.2012.13.3.161.

[71] J. Shah, M. Ranjan, P. Thareja, P. Estellé, Tailoring stability and thermophysical properties of CuO nanofluid through ultrasonication, J. Therm. Anal. Calorim. (2022). doi:10.1007/s10973-022-11266-y.

[72] S.U. Ilyas, R. Pendyala, M. Narahari, Rheological behavior of mechanically stabilized and surfactant-free MWCNT-thermal oil-based nanofluids, Int. Commun. Heat Mass Transf. 87 (2017). doi:10.1016/j.icheatmasstransfer.2017.07.015.

[73] L.U.R. Sica, E.M.C. Contreras, E.P. Bandarra Filho, J.A.R. Parise, An experimental viscosity investigation on the use of non-Newtonian graphene heat transfer nanofluids at below-ambient temperatures, Int. J. Energy Res. (2021). doi:10.1002/er.6675.

[74] N. Phan-Thien, Understanding Viscoelasticity - An Introduction to Rheology, Grad. Texts Phys. (2013).

[75] M. Afrand, D. Toghraie, B. Ruhani, Effects of temperature and nanoparticles concentration on rheological behavior of Fe3O4-Ag/EG hybrid nanofluid: An experimental study, Exp. Therm. Fluid Sci. 77 (2016) 38–44. doi:10.1016/j.expthermflusci.2016.04.007.

[76] D. Cabaleiro, M.J. Pastoriza-Gallego, C. Gracia-Fernández, M.M. Piñeiro, L. Lugo, Rheological and volumetric properties of TiO2-ethylene glycol nanofluids, Nanoscale Res. Lett. 8 (2013) 286. doi:10.1186/1556-276X-8-286.

[77] P. Coussot, Yield stress fluid flows: A review of experimental data, J. Nonnewton. Fluid Mech.

(2014). doi:10.1016/j.jnnfm.2014.05.006.

[78] J. Sobczak, J.P. Vallejo, J. Traciak, S. Hamze, J. Fal, P. Estellé, L. Lugo, G. Żyła, Thermophysical profile of ethylene glycol based nanofluids containing two types of carbon black nanoparticles with different specific surface areas, J. Mol. Liq. (2021). doi:10.1016/j.molliq.2020.115255.

[79] J.P. Vallejo, S. Gómez-Barreiro, D. Cabaleiro, C. Gracia-Fernández, J. Fernández-Seara, L. Lugo, Flow behaviour of suspensions of functionalized graphene nanoplatelets in propylene glycol–water mixtures, Int. Commun. Heat Mass Transf. 91 (2018) 150–157. doi:10.1016/j.icheatmasstransfer.2017.12.001.

[80] S. Hamze, D. Cabaleiro, T. Maré, B. Vigolo, P. Estellé, Shear flow behavior and dynamic viscosity of few-layer graphene nanofluids based on propylene glycol-water mixture, J. Mol. Liq. 316 (2020) 113875. doi:10.1016/j.molliq.2020.113875.

[81] S.U. Ilyas, R. Pendyala, M. Narahari, L. Susin, Stability, rheology and thermal analysis of functionalized alumina- thermal oil-based nanofluids for advanced cooling systems, Energy Convers. Manag. 142 (2017) 215–229. doi:10.1016/j.enconman.2017.01.079.

[82] A. Bakak, M. Lotfi, R. Heyd, A. Ammar, A. Koumina, Viscosity and rheological properties of graphene nanopowders nanofluids, Entropy. (2021). doi:10.3390/e23080979.

[83] H. Khodadadi, S. Aghakhani, H. Majd, R. Kalbasi, S. Wongwises, M. Afrand, A comprehensive review on rheological behavior of mono and hybrid nanofluids: Effective parameters and predictive correlations, Int. J. Heat Mass Transf. (2018). doi:10.1016/j.ijheatmasstransfer.2018.07.103.

[84] C. Ezekwem, A Recent Review of Viscosity Models for Nanofluids, Energy Sources, Part A Recover. Util. Environ. Eff. (2022). doi:10.1080/15567036.2021.1993469.

[85] A.K. Tiwari, N.S. Pandya, Z. Said, S.H. Chhatbar, Y.A. Al-Turki, A.R. Patel, 3S (Sonication, surfactant, stability) impact on the viscosity of hybrid nanofluid with different base fluids: An experimental study, J. Mol. Liq. (2021). doi:10.1016/j.molliq.2021.115455.

[86] M.N.A.W.M. Yazid, N.A.C. Sidik, W.J. Yahya, Heat and mass transfer characteristics of carbon nanotube nanofluids: A review, Renew. Sustain. Energy Rev. (2017). doi:10.1016/j.rser.2017.05.192.

[87] J.P. Vallejo, G. Żyła, J. Fernández-Seara, L. Lugo, Rheological behaviour of functionalized graphene nanoplatelet nanofluids based on water and propylene glycol:water mixtures, Int.

Commun. Heat Mass Transf. 99 (2018) 43–53. doi:10.1016/j.icheatmasstransfer.2018.10.001.